Chemical cycling and deposition of atmospheric mercury in Polar Regions: review of recent measurements and comparison with models

Hélène Angot[1], Ashu Dastoor[2], Francesco De Simone[3], Katarina Gårdfeldt[4], Christian N. Gencarelli[3], Ian M. Hedgecock[3], Sarka Langer[5], Olivier Magand[6, 1], Michelle N. Mastromonaco[4], Claus Nordstrøm[7], Katrine A. Pfaffhuber[8], Nicola Pirrone[9], Andrei Ryjkov[2], Noelle E. Selin[10, 11], Henrik Skov[7], Shaojie Song[10], Francesca Sprovieri[3], Alexandra Steffen[12], Kenjiro Toyota[12], Oleg Travnikov[13], Xin Yang[14], Aurélien Dommergue[1, 6]

[1]Univ. Grenoble Alpes, Laboratoire de Glaciologie et Géophysique de l'Environnement (LGGE), 38041 Grenoble, France

[2]Air Quality Research Division, Environment and Climate Change Canada, 2121 TransCanada Highway, Dorval, Quebec H9P 1J3, Canada

[3]CNR-Institute of Atmospheric Pollution Research, Division of Rende, UNICAL-Polifunzionale, 87036 Rende, Italy

[4]Department of Chemistry and Chemical Engineering, Chalmers University of Technology SE-412 96 Göteborg, Sweden

[5]IVL Swedish Environmental Research Institute, P.O. Box 530 21, 400 14 Göteborg, Sweden

[6]CNRS, Laboratoire de Glaciologie et Géophysique de l'Environnement (LGGE), 38041 Grenoble, France

[7]National Environmental Research Institute, Frederiksborgvej 399, 4000 Roskilde, Denmark

[8]Norwegian Institute for Air Research (NILU), P.O. Box 100, 2027 Kjeller, Norway

[9]CNR-Institute of Atmospheric Pollution Research, Area della Ricerca di Roma 1, Monterotondo, 00015 Rome, Italy

[10]Department of Earth, Atmospheric and Planetary Sciences, Massachusetts Institute of Technology, Cambridge, MA, USA

[11]Institute for Data, Systems, and Society, Massachusetts Institute of Technology, Cambridge, MA, USA

[12]Air Quality Research Division, Environment and Climate Change Canada, Toronto, Ontario M3H 5T4, Canada

[13]Meteorological Synthesizing Centre, East of EMEP, 2nd Roshchinsky proezd, 8/5, 115419 Moscow, Russia

[14]British Antarctic Survey, Cambridge, United Kingdom

Correspondence to: A. Dommergue (aurelien.dommergue@univ-grenoble-alpes.fr)

Abstract

Mercury (Hg) is a worldwide contaminant that can cause adverse health effects to wildlife and humans. While atmospheric modeling traces the link from emissions to deposition of Hg onto environmental surfaces, large uncertainties arise from our incomplete understanding of atmospheric processes (oxidation pathways, deposition, and reemission). Atmospheric Hg reactivity is exacerbated in high latitudes and there is still much to be learned from Polar Regions in terms of atmospheric processes. This paper provides a synthesis of the atmospheric Hg monitoring data available in recent years (2011-2015) in the Arctic and in Antarctica along with a comparison of these observations with numerical simulations using four cutting-edge global models. The cycle of atmospheric Hg in the Arctic and in Antarctica presents both similarities and differences. Coastal sites in the two regions are both influenced by springtime atmospheric Hg depletion events and by summertime snowpack reemission and oceanic evasion of Hg. The cycle of atmospheric Hg differs between the two regions primarily because of their different geography. While Arctic sites are significantly influenced by Northern Hemispheric Hg emissions especially in winter, coastal Antarctic sites are significantly influenced by the reactivity observed on the East Antarctic ice sheet due to katabatic winds. Based on the comparison of multi-model simulations with observations, this paper discusses whether the processes that affect atmospheric Hg seasonality and inter-annual variability are appropriately represented in the models, and identifies research gaps in our understanding of the atmospheric Hg cycling in high latitudes.

1 Introduction

Mercury (Hg) can be emitted to the atmosphere by natural geological sources (e.g., volcanic emissions) and a variety of anthropogenic activities (e.g., coal combustion, artisanal and small-scale gold mining) (UNEP, 2013a). The dominant form of atmospheric mercury is gaseous elemental mercury (Hg(0)) (Lindberg and Stratton, 1998). Hg(0) has an atmospheric lifetime of 0.5 to 1 year (Selin, 2009) and can therefore be transported worldwide. It can be oxidized into highly reactive and water soluble gaseous and particulate divalent species (Hg(II) and Hg(p), respectively) that can deposit onto environmental surfaces (e.g., land, surface oceans) through wet and dry processes (Lindqvist and Rodhe, 1985). Upon deposition, mercury can be reemitted to the atmosphere or converted – in aquatic systems – to methylmercury (Driscoll et al., 2013). Anthropogenic activities have altered the global geochemical cycle of mercury, enhancing the amount of mercury circulating in the atmosphere and surface oceans by at least a factor of three (Lamborg et al., 2014; Amos et al., 2015).

Methylmercury is a worldwide contaminant of seafood that can cause adverse effects on the developing nervous system of vulnerable populations (AMAP, 2015). The Minamata Convention on mercury – global treaty to protect human health and the environment from mercury – was opened for signature in October 2013 (UNEP, 2013b). To date, the Convention has been signed by 128 countries and ratified by 28. It will enter into force once it is ratified by 50 nations. As noted in the preamble of the Convention, Arctic ecosystems and indigenous communities are particularly vulnerable due to the biomagnification of mercury and contamination of traditional foods. In order to reduce mercury effects, the pathway from emissions to human and environmental impacts needs to be traced. Atmospheric modeling provides a first step by tracing the link from emissions to deposition onto environmental surfaces. Deposition of mercury in a particular region depends on the magnitude and speciation of domestic and foreign emissions, and on the oxidative capacity of the atmosphere that transforms Hg(0) to deposited divalent species (UNEP, 2015). Deposition is partly offset by the revolatilization of a fraction of deposited mercury. Large uncertainties associated with the models arise as a result of our incomplete understanding of atmospheric processes (e.g., oxidation pathways, deposition, and reemission) (Kwon and Selin, 2016). Atmospheric mercury reactivity is exacerbated in high latitudes and there is still much to be learned from Polar Regions in terms of atmospheric processes.

First discovered in 1995 (Schroeder et al., 1998), Atmospheric Mercury Depletion Events (AMDEs) are observed in springtime throughout the Arctic (Lindberg et al., 2001; Berg et al., 2003a; Poissant and Pilote, 2003; Skov et al., 2004; Steffen et al., 2005) as a result of the oxidation of Hg(0) by reactive bromine species (Lu et al., 2001; Brooks et al., 2006; Sommar et al., 2007). AMDEs can lead to a deposition of ~ 100 tons of mercury per year to the Arctic (Ariya et al., 2004; Skov et al., 2004; Dastoor et al., 2015). The fate of mercury deposited onto the snowpack during AMDEs is still a matter of debate in the scientific mercury community (Steffen et al., 2008). Several studies reported significant reemission (e.g., Ferrari et al., 2005; Brooks et al., 2006; Kirk et al., 2006; Sommar et al., 2007; Dommergue et al., 2010a) although a fraction of mercury may likely accumulate within the snowpack (Hirdman et al., 2009; Larose et al., 2010). While the Arctic has been extensively monitored – with hundreds of publications focusing on AMDEs, measurements are sporadic in Antarctica. To the best of the author's knowledge, only eleven studies dealing with atmospheric mercury in Antarctica (and using modern instrument) have been published (Ebinghaus et al., 2002; Sprovieri et al., 2002; Temme et al., 2003; Brooks et al., 2008a; Brooks et al., 2008b; Dommergue et al., 2012; Pfaffhuber et al., 2012; Angot et al., 2016a; Angot et al., 2016b; Nerentorp Mastromonaco et al., 2016; Wang et al., 2016). The earliest studies showed the occurrence of AMDEs in coastal Antarctica after polar sunrise. The latest studies highlighted new atmospheric processes in the Antarctic boundary layer – both in winter and summertime – leading to the formation and subsequent deposition of reactive mercury. In the meantime, several studies showed that the Antarctic Plateau plays a key role in influencing the cycle of atmospheric mercury at a continental scale.

The first objective of this paper is to provide a synthesis of the atmospheric mercury monitoring data available in recent years (2011-2015) in Polar Regions. Secondly, we provide a comparison of these observations with numerical simulations of atmospheric mercury concentrations using cutting-edge global models. Finally, this paper identifies research gaps in our understanding and modeling of the atmospheric mercury cycling in high latitudes.

2 Experimental Section

2.1 Measurements of atmospheric mercury species

2.1.1 Definitions

Hg(0), Hg(II), and Hg(p) are the most abundant mercury species in the atmosphere. Atmospheric Hg(0) is easily and accurately measured in Polar Regions (Steffen et al., 2008; Dommergue et al., 2010b). Hg(p) and Reactive Gaseous Mercury (RGM) – the latter consisting of various gaseous Hg(II) compounds – are operationally defined. Total Gaseous Mercury (TGM) refers to the sum of Hg(0) and Hg(II), and Reactive Mercury (RM) to the sum of RGM and Hg(p).

2.1.2 Instrumentation

Measurements of atmospheric mercury species were performed at various sites in the Arctic and in Antarctica over the 2011-2015 period (Fig. 1). All Hg(0) measurements reported in this paper were performed using a Tekran gas phase analyzer (Model 2537), and all RGM and Hg(p) measurements using a Tekran speciation unit (1130/1135) (Table 1). The Tekran 2537 analyzer is based on the amalgamation of mercury onto a gold cartridge followed by a thermal desorption and detection by an integrated cold vapor atomic fluorescence spectrometer (CVAFS) at 253.7 nm (Fitzgerald and Gill, 1979; Bloom and Fitzgerald, 1988). The analysis of Hg(0) is semi-continuous and the presence of two gold cartridges allows alternating sampling and desorption modes. At all sampling sites, the sample air stream was prefiltered either through a Tekran speciation unit or through a sodalime trap and/or a PTFE (polytetrafluoroethylene) filter (Table 1). Some researchers report ambient air collected at Polar sites as TGM (Ebinghaus et al., 2002), instead of Hg(0), but the PTFE filter on the front of the analyzer inlet most likely removes RGM and thus only Hg(0) is collected and analyzed (Steffen et al., 2002; Steffen et al., 2008). Due to the extremely cold and dry air in Antarctica, no heated sampling line was used and no sodalime was applied at TR, DC, and DDU. Collected at 5 to 15 min intervals at the various sites, Hg(0) measurements are reported here as hourly averages. RGM and Hg(p) measurements at ALT and ANT were performed using a Tekran speciation unit – connected to a 2537 analyzer through a PTFE heated sampling line – through a multistep procedure as described elsewhere (Lindberg et al., 2002) using an impactor inlet (2.5 µm cut-off aerodynamic diameter at 10 L min^{-1}), a KCl-coated quartz

annular denuder in the 1130 unit, and a quartz regenerable particulate filter (RPF) in the 1135 unit.

Quality assurance and quality control procedures

Auto-calibrations of the 2537 analyzers were performed every 25 to 72 hours at the various sites using an internal mercury permeation source. The accuracy of this permeation source was checked at least once per year against manual injections using a Tekran 2505 mercury vapor calibration unit and following a strict procedure adapted from Dumarey et al. (1985). The detection limit for Hg(0) measurements is 0.10 ng m^{-3} according to the instrument manual (Tekran, 2011). Based on experimental evidence, the average systematic uncertainty for Hg(0) measurements is of ~ 10 % (Slemr et al., 2015). There is no robust calibration technique of the Tekran speciation unit and no certified reference material available. There is growing evidence that RGM and Hg(p) might suffer from significant biases and interferences (Lyman et al., 2010; Gustin et al., 2013; Jaffe et al., 2014; Huang et al., 2013; Kos et al., 2013), and that RGM concentrations might be underestimated by as much as a factor of 2 - 13 (Gustin et al., 2016). Despite these limitations, the Tekran speciation unit is currently the best available automated method, and Hg(p) and RGM measurements can be used as first estimates to evaluate atmospheric models. Maintenance operations on the Tekran 2537/1130/1135 instruments and screening criteria for data validation/invalidation were performed according to the directives of the standard operational procedure (SOP) from CAMNet (Canadian Mercury Measurement Network), AMNet (United States Atmospheric Mercury Network), or GMOS (Global Mercury Observation System) (Steffen et al., 2012; D'Amore et al., 2015).

2.2 Global mercury simulations

The current study is based on multi-model simulations performed as part of the Mercury Modeling Task Force (MMTF) under the GMOS project (Travnikov et al., in preparation). Four global models (ECHMERIT, GEM-MACH-Hg, GEOS-Chem, and GLEMOS) were applied for evaluating monthly-averaged atmospheric mercury concentrations and deposition at various Arctic and Antarctic ground-based sites for the year 2013. Additionally, GEM-MACH-Hg and GEOS-Chem provided hourly-averaged data from 2011 to 2014 to allow investigations of inter-annual variability. A brief description of the parameterization of the four models is given below. The models differ significantly in their description of mercury

atmospheric chemistry and their parameterization of processes specific to Polar Regions (i.e., AMDEs, oceanic evasion, and re-emissions from the snowpack).

2.2.1 ECHMERIT

ECHMERIT is a fully-coupled model, based on the Atmospheric General Circulation Model (AGCM) ECHAM5, and a mercury chemistry module, developed at the Institute for Atmospheric Pollution of the National Research Council (CNR-IIA) of Italy (Jung et al., 2009; De Simone et al., 2014; De Simone et al., 2016). The base mechanism includes oxidation of Hg(0) by OH and O_3 in the gas and aqueous (in-cloud) phases (reactions R1 to R3). Rate constants of reactions (R1) to (R3) are from Sommar et al. (2001), Hall (1995), and Munthe (1992), respectively.

$$Hg(0) + OH \rightarrow Hg(II) \quad \textbf{(R1)}$$

$$Hg(0) + O_3 \rightarrow Hg(II) \quad \textbf{(R2)}$$

$$Hg(0)_{(aq)} + O_{3_{(aq)}} \rightarrow Hg(II)_{(aq)} \quad \textbf{(R3)}$$

Oxidant fields (OH/O_3) are imported from MOZART (Model for Ozone and Related Chemical Tracers) (Emmons et al., 2010). In the base run used for this work bromine chemistry is not included, and there is no parameterization of AMDEs. ECHMERIT implements dynamically calculated ocean emissions for all ice-free basins, including Polar Regions, as described in De Simone et al. (2014), and a prompt re-emission of 60 % of deposited mercury over ice (Selin et al., 2008).

2.2.2 GEM-MACH-Hg

GEM-MACH-Hg is a mercury version of the Environment and Climate Change Canada's (ECCC's) current operational air quality forecast model – Global Environmental Multi-scale – Modelling air quality and Chemistry (GEM-MACH). GEM-MACH-Hg is an on-line model, meaning that the meteorology is simulated in-step with the chemistry, and includes representation of physicochemical processes of mercury based on the ECCC's previous mercury model – GRAHM (Dastoor and Larocque, 2004; Dastoor et al., 2008; Durnford et al., 2010; Durnford et al., 2012; Kos et al., 2013; Dastoor et al., 2015). The horizontal resolution of the model for this study is $1° \times 1°$ latitude/longitude. Hg(0) is oxidized in the atmosphere by OH (R1) and bromine (reactions (R4) to (R6), X = Br or BrO). The rate constant of (R1) is from Sommar et al. (2001), but scaled down by a coefficient of 0.34 to take into account possible dissociation reactions (Tossell, 2003; Goodsite et al., 2004). Rate

constants of reactions (R4) to (R6) are from Donohoue et al. (2006), Dibble et al. (2012), and Goodsite et al. (2004), respectively. Aqueous-phase reduction reactions are not included.

$$Hg(0) + Br \rightarrow Hg(I)Br \qquad \textbf{(R4)}$$

$$Hg(I)Br \rightarrow Hg(0) + Br \qquad \textbf{(R5)}$$

$$Hg(I)Br + X \rightarrow Hg(II)X \qquad \textbf{(R6)}$$

OH fields are from MOZART (Emmons et al., 2010) while BrO is derived from 2007-2009 satellite observations of BrO vertical columns. The associated Br concentration is then calculated from photochemical steady state according to equation (1), where J_{BrO} is the BrO photolysis frequency, and $k_1 = 2.1\ 10^{-11}$ cm^3 molecule^{-1} s^{-1} and $k_2 = 1.2\ 10^{-12}$ cm^3 molecule^{-1} s^{-1} are the rate coefficients for the $BrO + NO \rightarrow Br + NO_2$ and $Br + O_3 \rightarrow BrO + O_2$ reactions, respectively (Platt and Janssen, 1995).

$$\frac{[Br]}{[BrO]} = \frac{J_{BrO} + k_1\,[NO]}{k_2\,[O_3]} \qquad \textbf{(1)}$$

Durnford et al. (2012) developed and implemented a dynamic multilayer snowpack/meltwater parameterization allowing the representation of deposition and reemission of mercury. Oceanic evasion of Hg(0) is activated if there is open water and the temperature at the air-sea interface is -4 °C or greater (Dastoor and Durnford, 2014). In addition, Hg(0) released from sea ice melting is also taken into account. The parameterization of AMDEs is based on Br production and chemistry, and snow reemission of Hg(0) (Dastoor et al., 2008).

2.2.3 GEOS-Chem

GEOS-Chem (v9-02) is a global chemical transport model driven by assimilated meteorological data from the NASA GMAO Goddard Earth Observing System (Bey et al., 2001). It couples a 3-D atmosphere (Holmes et al., 2010), a 2-D mixed layer slab ocean (Soerensen et al., 2010), and a 2-D terrestrial reservoir (Selin et al., 2008) with a horizontal resolution of $2° \times 2.5°$ latitude/longitude. Three mercury tracers (Hg(0), Hg(II), and Hg(p)) are tracked in the atmosphere (Amos et al., 2012). Mercury fluxes at terrestrial and ocean surfaces are described in Song et al. (2015). A two-step oxidation mechanism initialized by Br atoms is used (reactions (R4) to (R6), X = Br or OH). Br fields are archived from a full-chemistry GEOS-Chem simulation (Parrella et al., 2012) while rate constants of reactions (R4) to (R6) are from Donohoue et al. (2006), Balabanov et al. (2005), and Goodsite et al. (2012), respectively. Some model setups related to Polar Regions are implemented in v9-02 of

the model as described in details in Holmes et al. (2010). 5 pptv of BrO – at the low end of concentrations reported by Neuman et al. (2010) – is added in the springtime Arctic (Antarctic) boundary layer during March-May (August-October) over areas with sea ice, sunlight, stable conditions, and temperatures below -5 °C. The associated Br concentration is then calculated from photochemical steady state according to equation (1) assuming that O_3 is depleted to 2 ppbv. Additionally, a snowpack reservoir is added. It accumulates deposited mercury and releases it as Hg(0) under sunlit conditions in a temperature-dependent way.

2.2.4 GLEMOS

GLEMOS (Global EMEP Multi-media Modelling System) is a multi-scale chemical transport model developed for the simulation of environmental dispersion and cycling of different chemicals including mercury (Travnikov and Ilyin, 2009). The model simulates atmospheric transport, chemical transformations and deposition of three mercury species (Hg(0), Hg(II), and Hg(p)). The atmospheric transport of tracers is driven by meteorological fields generated by the Weather Research and Forecast (WRF) modelling system (Skamarock et al., 2007) fed by the operational analysis data from ECMWF. The model in the base configuration has a horizontal resolution of $1° \times 1°$. The base mechanism includes oxidation of Hg(0) by OH (R1) and O_3 (R2) in the atmosphere. Rate constants are from Sommar et al. (2001) and Hall (1995), respectively. The model also includes in-cloud oxidation of Hg(0) by OH, O_3, and Cl with associated rate constants from Gårdfeldt et al. (2001), Munthe (1992), and Lin and Pehkonen (1999), respectively. In-cloud reduction by SO_3^{2-} is also implemented, with an associated rate constant from Petersen et al. (1998). Reactant fields are imported from MOZART (Emmons et al., 2010).

The parameterization of AMDEs in Polar Regions is based on Br chemistry following the two-step mechanism (R4)-(R6) described in Holmes et al. (2010). Br concentrations are extracted from p-TOMCAT (parallel-Tropospheric Off-Line Model of Chemistry and Transport) results (Yang et al., 2005). GLEMOS includes an empirical parameterization of prompt-reemission from snow. It is assumed that reemission occurs only from newly deposited mercury in the presence of solar radiation. Two competing processes are considered: photoreduction and ageing of deposited mercury with the characteristic times of 1 day and 10 days, respectively. It is also assumed that all reduced mercury is immediately reemitted back to the atmosphere. The aged fraction of mercury does not undergo reduction and is accumulated within the snowpack. No mercury evasion from the ocean is implemented.

2.3 Goodness-of-fit statistics between modeled and observed data

The Nash-Sutcliffe efficiency (NSE, Nash and Sutcliffe, 1970) indicates how well the plot of observed versus simulated data fits the 1:1 line – NSE = 1 corresponding to the perfect match. NSE is defined as one minus the sum of the absolute squared differences between the simulated and observed values normalized by the variance of the observed values:

$$\text{NSE} = 1 - \frac{\sum_{i=1}^{N}(O_i - S_i)^2}{\sum_{i=1}^{N}(O_i - \bar{O})^2} \qquad \textbf{(2)}$$

The root mean square error (RMSE) gives the standard deviation of the model prediction error (in the same units of simulated and observed values). A smaller value indicates better model performance. It is calculated as follows:

$$\text{RMSE} = \sqrt{\frac{1}{N} \sum_{i=1}^{N}(S_i - O_i)^2} \qquad \textbf{(3)}$$

The percent bias (PBIAS, in %) measures the average tendency of the simulated values to be larger or smaller than their observed ones. The optimal value of PBIAS is 0. PBIAS is calculated as follows:

$$\text{PBIAS} = 100 \frac{\sum_{i=1}^{N}(S_i - O_i)}{\sum_{i=1}^{N} O_i} \qquad \textbf{(4)}$$

NSE, RMSE, and PBIAS were calculated by using the R package "hydroGOF" (Zambrano-Bigiarini, 2014).

3 Results and Discussion

3.1 Arctic sites

3.1.1 Observations

Fig. 2a shows monthly box plots of all data collected at the four Arctic sites. The average Hg(0) value in the Arctic over the 2011-2014 period is 1.46 ± 0.33 ng m^{-3}. This concentration falls within the range of what is observed in the Northern Hemisphere (Sprovieri et al., 2016b). The highest mean is at AND (1.55 ± 0.15 ng m^{-3} over the 2011-2015 period), which is closer from European industrialized areas than other sites and experiences less frequent and pronounced AMDEs in spring (see section 3.1.1.2). There is a clear Hg(0) concentration gradient (except from June to August): AND > NYA > SND > ALT.

The Hg(0) concentration data from the four Arctic sites for the period 2011-2015 are presented as monthly box and whisker plots in Fig. 3. Information regarding annually- and monthly-based statistics at the three sites can be found in Tables 2 and 3, respectively. The annual medians at NYA and AND (Table 2) suggest a low inter annual variability in the distribution of Hg(0) concentrations. Conversely, there is a high degree of inter-annual variability at ALT and SND driven by the intensity of spring and summertime processes. This will be addressed in the following sections.

The mean seasonal variation of Hg(0) concentrations at ground-based Arctic sites is displayed in Fig. 4a. Summer refers to June-August, fall to September-November, winter to December-February, and spring to March-May. Hg(0) concentrations exhibit a strong and consistent seasonal pattern year after year, as already reported by others (Steffen et al., 2005; Berg et al., 2013). Hg(0) concentrations reach a distinct maximum in summer at ALT, SND, and NYA (mean concentrations of 1.63 ± 0.37, 1.63 ± 0.37, and 1.60 ± 0.23 ng m^{-3}, respectively). In late summer the concentrations start to decrease and reach in fall a mean value of 1.28 ± 0.12 ng m^{-3} at ALT, 1.36 ± 0.11 ng m^{-3} at SND, and 1.46 ± 0.16 ng m^{-3} at NYA. In winter, concentrations increase slightly and are significantly higher than in fall at the three sites (*p* value < 0.0001 at the three sites, Mann-Whitney test). Springtime reflects the lowest Hg(0) concentrations with mean values of 1.11 ± 0.58 ng m^{-3} at ALT, 1.28 ± 0.51 ng m^{-3} at SND, and 1.38 ± 0.38 ng m^{-3} at NYA. The seasonal cycle is more pronounced at ALT than at SND and NYA. In contrast, lower concentrations were found in the Chukchi Sea in July (1.17 ± 0.38 ng m^{-3}) than in September (1.51 ± 0.79 ng m^{-3}) during the CHINARE 2012 expedition (Yu et al., 2014).

Hg(0) concentrations at AND exhibit an opposite seasonal cycle with a significantly (*p* value < 0.0001, Mann-Whitney test) higher mean concentration in winter (1.67 ± 0.11 ng m^{-3}) than in summer (1.48 ± 0.12 ng m^{-3}), in line with the seasonality reported at Pallas, Finland (67°22'N, 26°39'E) (Berg et al., 2001; Sprovieri et al., 2016b). The mechanisms which cause the seasonal variation of Hg(0) concentrations at Arctic sites are discussed in the following sections.

3.1.1.1 Wintertime advection of Hg from mid-latitudes

Several studies highlighted that the Arctic is significantly influenced by atmospheric pollution from mid-latitudes – phenomenon known as Arctic haze – during wintertime (Barrie et al., 1981; Heintzenberg et al., 1981; Shaw, 1982; Heidam et al., 1999; Heidam et al., 2004; Bourgeois and Bey, 2011; Nguyen et al., 2013). Dastoor and Larocque (2004) used an on-line

model to explain the observed seasonal variations in atmospheric mercury circulation and showed frequent episodes of mercury transport from mid-latitudes sources to the Arctic in winter. Similarly, Hirdman et al. (2009) attributed the highest 10 % of all wintertime Hg(0) data at NYA to transport of air masses especially from Europe. Higher Hg(0) concentrations in winter compared to fall at ALT, SND, and NYA can therefore be attributed to the meteorological differences in the seasonal circulation patterns (Dastoor and Larocque, 2004). Higher concentrations in winter at AND compared to the three other Arctic sites can be attributed to the powerful advection of air masses from Europe at this site (Durnford et al., 2010).

3.1.1.2 Springtime AMDEs

AMDEs in the Arctic are defined as Hg(0) concentrations below 1.00 ng m^{-3} (Steffen et al., 2005; Cobbett et al., 2007). Based on this threshold, AMDEs occur in 39 %, 28 %, 15 %, and 1 % of the 2011-2014 springtime observations at ALT, SND, NYA, and AND, respectively. The fact that ALT experiences stronger and more frequent AMDEs than other Arctic sites could be due to air masses circulation patterns. Several studies indicated that a large fraction of the AMDEs reported at NYA and AND are suspected to result from the long-range transport of air masses containing depleted Hg(0) from areas over the Arctic Ocean (Gauchard et al., 2005; Sommar et al., 2007; Berg et al., 2008; Steen et al., 2011; Berg et al., 2013). A statistical analysis on the results from a Lagrangian particle dispersion model (FLEXPART) and Hg(0) concentrations measured at NYA was performed by Hirdman et al. (2009) to identify source regions of high- and low-Hg air masses. The authors concluded that the lowest 10 % of the Hg(0) data at NYA in spring were strongly associated with transport across the sea-ice covered Arctic Ocean at low altitudes – areas where elevated BrO concentrations are seen in the atmospheric column by satellite observations (e.g., Lindberg et al., 2002). Similarly, a correlation of AMDEs with wind direction at ALT supports the origin of depletion events over the Arctic Ocean (Cole and Steffen, 2010). The less frequent and pronounced AMDEs at AND may be explained by the fact that this site is farther away from the source areas of AMDEs (Berg et al., 2008).

Over the 2011-2015 period, AMDEs at NYA are evenly distributed between April and May (38 % of the time in both cases), and fewer in March and June (14 and 10 % of the time, respectively). This result is in good agreement with the distribution reported by Berg et al. (2013) over the 2000-2009 period. Conversely, AMDEs are more frequent in April (41 %) than in May (32 %) at ALT, while less frequent in April (34 %) than in May (43 %) at SND.

Interestingly, the analysis of the ALT dataset from 1995 to 2007 by Cole and Steffen (2010) revealed that, over time, the month of maximum AMDE activity shifted from May to April. On the contrary, the analysis of the NYA dataset from 2000 to 2009 by Berg et al. (2013) did not evidence such a change in the timing of AMDEs. The reason for this shift in timing of AMDEs at ALT is not fully understood but could be due to local meteorology (Cole and Steffen, 2010). The authors found that the length, magnitude, and frequency of AMDEs decreased with increasing local temperature. These results are consistent with earlier studies on the temperature dependence of the halogen chemistry initiating AMDEs and ozone depletion events (Koop et al., 2000; Adams et al., 2002; Tarasick and Bottenheim, 2002; Sander et al., 2006) and with a modeling study reporting that increasing surface air temperature decreases the frequency of AMDEs (Chen et al., 2015) . However, considering the fact that AMDEs observed at Arctic sites often result from the transport of depleted air masses, local temperature might not be the key explanatory parameter. Moore et al. (2014) showed that AMDEs and ozone depletion events near Barrow, Alaska, are directly linked to sea-ice dynamics. According to the authors, depletion events are favored by consolidated sea-ice cover but both Hg(0) and O_3 concentrations immediately recover to near-background concentrations when air masses cross open leads within a day before measurements. The authors attributed this recovery of concentrations to changes in boundary-layer dynamics induced by sea-ice leads, causing significant convective mixing with non-depleted air masses aloft. Further work is needed to establish the degree to which sea-ice dynamics across the Arctic might influence the inter-annual variability of AMDEs at the various Arctic sites. Indeed, AMDEs occurred at ALT in 36 % (2011), 51 % (2012), 50 % (2013), and 21 % (2014) of the springtime observations, at SND in 37 % (2011), 16 % (2012), 36 % (2013), and 19 % (2014) of the springtime observations, and finally at NYA in 18 % (2011), 13 % (2012), 16 % (2013), 20 % (2014), and 6 % (2015) of the springtime observations.

Several studies reported RGM and Hg(p) concentrations during AMDEs at Arctic sites (Lindberg et al., 2002; Berg et al., 2003a; Steffen et al., 2003; Aspmo et al., 2005; Gauchard et al., 2005; Sprovieri et al., 2005a; Steen et al., 2011; Wang, 2015). Fig. 5 shows box plots of the monthly concentrations of RGM and Hg(p) at ALT over the 2011-2014 period. A distinct annual cycle is highlighted in this figure. Hg(p) concentrations increase from November through February likely due to the Arctic haze (Steffen et al., 2014), reach a maximum in March and April due to AMDEs, and then decrease. RGM concentrations peak in spring and then gradually decrease. The production of RGM in June and July – after the

AMDEs season – is observed every year and remains unexplained (Steffen et al., 2014). While Hg(p) is the dominant species in early spring, a clear shift is observed, from the predominance of Hg(p) to RGM in AMDEs occurring toward the end of spring. This shift has already been evidenced at Churchill, Manitoba (Kirk et al., 2006), ALT (Cobbett et al., 2007), and NYA (Steen et al., 2011), and has been shown to repeat year after year at ALT (Steffen et al., 2014). Steffen et al. (2014) suggested that this shift is due to temperature and particle availability. Using a detailed air-snowpack model for interactions of bromine, ozone, and mercury in the springtime Arctic, Toyota et al. (2014) proposed that Hg(p) is mainly produced as $HgBr_4^{2-}$ through uptake of RGM into bromine-enriched aerosols after ozone is significantly depleted in the air mass. In addition, Toyota et al. (2014) provided the temperature dependence of these reactions which needs to be verified experimentally. Based on ten years of data, Steffen et al. (2014) also reported higher levels of mercury in the snow when the atmospheric conditions favored the formation of RGM. This springtime shift from the predominance of Hg(p) to RGM in AMDEs likely directly impacts the amount of mercury deposited onto the snowpack. This will be further discussed in section 3.1.2.2.

3.1.1.3 Summer enhancement of Hg(0) concentrations

According to Dastoor and Larocque (2004), advection of mercury from mid-latitudes to the Arctic is insignificant in summer due to weak airflow movements and to a confined polar front. The increase of Hg(0) concentrations in summer could be due to the reemission of mercury deposited during springtime AMDEs. However, the comparison of the magnitude of the springtime depletion and the magnitude of the summer enhancement at ALT suggests otherwise. Mean springtime Hg(0) concentrations are lower – suggesting more intense and/or frequent AMDEs – in 2012 (0.97 ± 0.53 ng m^{-3}) and 2013 (0.89 ± 0.57 ng m^{-3}) than in 2011 (1.19 ± 0.59 ng m^{-3}) and 2014 (1.37 ± 0.50 ng m^{-3}), while mean summertime concentrations are higher – suggesting more reemission – in 2011 (1.81 ± 0.37 ng m^{-3}) and 2014 (1.63 ± 0.31 ng m^{-3}) than in 2012 (1.43 ± 0.27 ng m^{-3}) and 2013 (1.65 ± 0.41 ng m^{-3}). Therefore, the summer enhancement of Hg(0) concentrations is generally attributed to emissions from snow and ice surfaces (Poulain et al., 2004; Sprovieri et al., 2005b; Sprovieri et al., 2005a; Sprovieri et al., 2010; Douglas et al., 2012) and/or to evasion from the ice-free surface waters of the Arctic Ocean (Aspmo et al., 2006; Andersson et al., 2008; Hirdman et al., 2009; Fisher et al., 2013; Dastoor and Durnford, 2014; Yu et al., 2014; Soerensen et al., 2016). Inhomogeneous distributions of Hg(0) were observed over the Arctic Ocean during the CHINARE 2012 (Yu et al., 2014) and the Beringia 2005 (Sommar et al., 2010) expeditions.

Both studies reported a rapid increase of concentrations in air when entering the ice-covered waters, highlighting the influence of sea ice dynamics on Hg(0) concentrations. The atmospheric mercury model (GRAHM) used by Dastoor and Durnford (2014) simulated a first peak in Hg(0) concentrations driven by revolatilization from snowpack/meltwaters, followed by a second peak driven by oceanic evasion – the timing of the peaks varying with location and year. Additional field and modeling studies suggested that some of the mercury in surface ocean waters may come from riverine input (Fisher et al., 2012; Yu et al., 2014; Soerensen et al., 2016).

As can be seen in Fig. 3, Hg(0) concentrations are significantly higher (p value < 0.0001, Mann-Whitney test) during summer 2011 at ALT (1.81 ± 0.37 ng m^{-3}) than during the following summers (1.57 ± 0.35 ng m^{-3} in average). At SND, Hg(0) concentrations peak in summer 2013 (1.91 ± 0.37 ng m^{-3} *vs.* 1.52 ± 0.26 ng m^{-3} in average during summers 2011, 2012, and 2014). One possible explanation for this inter-annual variability is sea ice extent. Daily sea ice maps can be obtained from http://www.iup.uni-bremen.de/iuppage/psa/2001/amsrop.html (Spreen et al., 2008). ALT and SND are both surrounded by multi-year ice. During summer 2011, the Hall Basin – waterway between Greenland and Canada's northernmost island where ALT is located – was ice-free. During summer 2013, sea ice extent was particularly low in the Greenland Sea – between Greenland and the Svalbard archipelago. These large areas of ice-free surface waters might have led to enhanced oceanic evasion near ALT, and SND in 2011 and 2013, respectively. Indeed, Yu et al. (2014) reported a negative correlation between TGM and salinity over an Arctic ice-covered region, suggesting that ice melting would enhance TGM concentrations. This hypothesis is further supported by wind data obtainable from http://climate.weather.gc.ca/historical_data/search_historic_data_e.html and http://villumresearchstation.dk/data/. At ALT, the summertime dominant wind direction is from north-east but with frequent and strong winds from south/south-west (Hall Basin), in line with results reported by Bilello (1973) and Cobbett et al. (2007). At SND, the dominant wind direction is from south-west but the direction becomes more variable in summer with winds also occurring from south and east (Bilello, 1973; Nguyen et al., 2013). Yet a comprehensive and systematic analysis of air masses back-trajectories and sea-ice extent is required to further investigate parameters responsible for the observed inter-annual variability.

NYA is normally surrounded by open water in the summer. Therefore, oceanic emissions are expected to act as a significant local source to NYA, while being a regional and diffuse source

at ALT and SND (Cole et al., 2013). However, the summer enhancement of Hg(0) concentrations is weaker at NYA than at ALT and SND (Fig. 4a). The western coast of Spitsbergen island, where NYA is located, was ice-free year-round over the period of interest possibly preventing the build-up of mercury-enriched ice-covered surface waters in winter and intense evasion in summer. Additionally, a comparative study was carried out at NYA with measurements at both 12 m a.s.l. and 474 m a.s.l.. While Aspmo et al. (2005) found no significant difference between Hg(0) concentrations at the two elevations, several studies (Berg et al., 2003b; Sprovieri et al., 2005b; Sommar et al., 2007) reported that Hg(0) concentrations at 12 m a.s.l. were higher in magnitude and exhibited a higher variability than at 474 m a.s.l.. Evidence of volatile mercury evasion from snow and water surfaces was also obtained, suggesting a cycling of mercury near the surface. Zeppelin station at 474 m a.s.l. is typically positioned over or at the top of the marine boundary layer of the fjord valley (Sommar et al., 2007) likely, at least partly, explaining why the summer enhancement of Hg(0) concentrations is weaker at NYA.

In contrast to observations at ALT, SND, and NYA, Hg(0) concentrations reach a minimum in summer at AND. Transport of air masses from Europe is dominant at AND (Durnford et al., 2010) and could mask any variability induced by oceanic evasion. The mean Hg(0) concentration in summer at AND (1.48 ± 0.12 ng m^{-3} over the 2011-2015 period) is consistent with the value of ~ 1.42 ng m^{-3} reported at Pallas, Finland over the 2013-2014 period (Sprovieri et al., 2016b).

3.1.2 Comparison with models

Table 4 displays goodness-of-fit statistics between monthly-averaged modeled and observed data in 2013. Except at ALT, modeled Hg(0) concentrations are biased-low suggesting that the four global models tend to underestimate sources of Hg(0). The ability of the four models to reproduce the observed seasonality of Hg(0) concentrations at Arctic sites in 2013 is shown in Fig. 6a and discussed in the following sections. As mentioned in section 2.2, GEM-MACH-Hg and GEOS-Chem provided hourly-averaged data from 2011 to 2014. The inter-annual variability of the monthly Hg(0) concentration distribution at Arctic sites as simulated by the two models is displayed in Fig. 7a while Table 5 shows the percent bias between hourly-averaged modeled and observed data on a seasonal basis from 2011 to 2014.

3.1.2.1 Seasonal variation

a) Winter

All the models (except ECHMERIT) overestimate Hg(0) concentrations at ALT in January and February 2013, but reproduce well the average value in December 2013 (Fig. 6a). It is worth noting that the observed mean value in January/February 2013 (1.24 ± 0.13 ng m^{-3}) is lower than the value observed in December 2013 (1.45 ± 0.07 ng m^{-3}) and lower than the hemispheric background (1.30 – 1.60 ng m^{-3} according to Sprovieri et al. (2016b)). Additionally, the observed mean value in January/February 2013 is at the low end of values reported at this period of the year at ALT from 2011 to 2014 (Fig. 3, 1.40 ± 0.16 ng m^{-3} in 2011, 1.32 ± 0.09 ng m^{-3} in 2012, and 1.47 ± 0.12 ng m^{-3} in 2014). The inter-annual variability of observed Hg(0) concentrations at ALT is not captured by models. Modeled Hg(0) concentrations in January/February range from 1.48 ± 0.03 in 2014 to 1.54 ± 0.03 ng m^{-3} in 2011 and 2012 with GEOS-Chem and from 1.54 ± 0.06 in 2012 to 1.58 ± 0.04 ng m^{-3} in 2013 with GEM-MACH-Hg. Similarly, the inter-annual variability of modeled Hg(0) concentrations is low at other Arctic sites (Fig. 7a). The wintertime inter-annual variability of observed Hg(0) concentrations might be driven by meteorology and mercury emissions in mid-latitudes. However, the AMAP/UNEP (2010) global inventory of mercury anthropogenic emissions (annual mean emission fields) was used for all simulated years (2011-2014) in both GEOS-Chem and GEM-MACH-Hg, preventing the consideration of inter-annual changes in anthropogenic emissions.

b) Spring

Springtime reflects the lowest Hg(0) concentrations at ALT, SND, and NYA due to the occurrence of AMDEs (see section 3.1.1.2). This minimum is well reproduced by GEM-MACH-Hg, GEOS-Chem, and GLEMOS at all three stations, but not reproduced by ECHMERIT (Fig. 6a). It should be noted that there is no parameterization of AMDEs in the latter. Interestingly, GLEMOS predicts a similar springtime minimum at AND in contradiction with the seasonal pattern observed at this station (see section 3.1.1.2). This discrepancy can likely be attributed to uncertainties in Br fields extracted from p-TOMCAT.

As discussed in section 3.1.1.2, AMDEs were less frequent at ALT in 2014. This lower occurrence frequency is fairly well reproduced by GEM-MACH-Hg (61 % (2011), 43 % (2012), 53 % (2013), and 36 % (2014)), but not at all by GEOS-Chem (4 % (2011), 6 % (2012), 13 % (2013), and 37 % (2014)). A temperature-dependence of BrO concentrations is implemented in GEM-MACH-Hg and Br_2 is assumed to occur only over consolidated sea-ice which would change with changing meteorological conditions. Conversely, a constant value of 5 pptv of BrO is added in the springtime Arctic boundary layer into GEOS-Chem v9-02.

However, updates to Arctic mercury processes will be implemented in v11-01 based on Fisher et al. (2012) and Fisher et al. (2013) (http://wiki.seas.harvard.edu/geos-chem/index.php/Mercury#Updates_to_Arctic_Hg_processes). BrO concentrations will depend on temperature according to a relationship chosen to optimize spring Hg(0) concentrations and the shift of peak depletion at ALT from May to April (see section 3.1.1.2). It should also be noted that GEOS-Chem relies on GEOS-5 and GEOS-FP meteorological fields in 2011-2013 and 2014, respectively. Simulations in Polar Regions can be very sensitive to subtle changes in meteorological fields, especially during the AMDEs season, which could at least partly explain the inter-annual variability of modeled AMDEs occurrence frequencies.

Based on the work by Moore et al. (2014) showing the impact of sea-ice leads on AMDEs (AMDEs might be favored by consolidated sea-ice cover, see section 3.1.1.2), real-time distribution of sea-ice dynamics including presence of leads is needed. Contrarily to conclusions by Moore et al. (2014), a recent modeling study (Chen et al., 2015) carried out using GEOS-Chem v9-02 – but including an ice/snow module and riverine inputs as described by Fisher et al. (2012) and Fisher et al. (2013) – showed that increasing sea ice lead occurrence increases the frequency of AMDEs. These contradictory results highlight the fact that further work is needed regarding the degree to which sea-ice dynamics across the Arctic alters mercury chemistry in spring.

c) Summer

All the models (except ECHMERIT in which polar processes are not implemented) capture, to some extent, the summertime Hg(0) enhancement. GLEMOS clearly underestimates summertime mean concentrations at ALT and SND (Fig. 6a). This can be attributed to missing reemissions and/or oceanic evasion. As mentioned is section 3.1.1.3, Dastoor and Durnford (2014) suggested two distinct summertime maxima: a first one supported by revolatilization from snowpack/meltwaters occurring from the end of May to mid-June at ALT, and in June at NYA; a second one supported by oceanic evasion from mid-July to early August at ALT and NYA. GEOS-Chem gives a summer maximum in June instead of July at ALT, SND, and NYA. This time-lag might result from to the fact that oceanic evasion from the Arctic Ocean is not implemented in v9-02. v11-01 of the model will include, among other updates, new present-day (2009) fields for net primary productivity (NPP) based on Jin et al. (2012), a UV-B dependence for Hg(II) reduction in seawater based on results of O'Driscoll et al. (2006), updated Hg(0) emissions from snow, and a source of mercury from the snowpack

to the Arctic Ocean at the onset of snowmelt. In order for the models to reproduce the inter-annual variability of Hg(0) concentrations, real-time distribution of areas of ice-free surface waters along with the type of surface (ice/snow/snow-free bedrock) are needed.

3.1.2.2 Reactive Mercury and deposition

Year 2013 modeled monthly-averaged RM concentrations and wet/dry deposition are displayed in Fig. 8a. GEOS-Chem, GEM-MACH-Hg, and GLEMOS predict increased RM concentrations in spring, during the AMDEs season, consistent with the observed pattern at ALT (Fig. 5) and NYA (Wang, 2015). The fact that ECHMERIT does not capture the spring enhancement is not surprising since the model does not implement any chemistry specific to Polar Regions. GLEMOS also predicts a RM spring maximum at AND, in line with the modeled Hg(0) spring minimum at this site (Fig. 6a). As discussed in section 3.1.2.1.b, this can likely be attributed to uncertainties in Br fields extracted from p-TOMCAT. Long-term measurements of RM in the Arctic are scarce and limited to ALT and NYA (data not presented here). According to Fig. 8a, all four models underestimate RM concentrations at ALT from at least January to April 2013. Similarly, the comparison of modeled RM concentrations at NYA with annual averages reported by Steen et al. (2011) and Wang (2015) suggest an underestimation of the concentrations by GEOS-Chem, GEM-MACH-Hg, and ECHMERIT.

According to the models, deposition of mercury peaks in spring at ALT and SND, consistent with the RM spring maximum. The deposition of mercury during AMDEs depends on temperature, relative humidity and aerosol contribution (Cobbett et al., 2007), and is higher when the atmospheric conditions favor the formation of RGM over Hg(p) (see section 3.1.1.2). Therefore, as suggested by Steffen et al. (2015), prevailing atmospheric conditions must be fully characterized in order to accurately evaluate the deposition of mercury. GEOS-Chem and GLEMOS both predict higher dry deposition in spring at NYA. Wet deposition is largely driven by precipitation – RM being readily scavenged by rain or snow, whereas dry deposition depends on the boundary layer stability and the type of the underlying surface (Cadle, 1991). Deposition of mercury in the Arctic is typically inferred from concentrations of total mercury in the snowpack (e.g., Steffen et al., 2014) or from a Hg(0) flux gradient method (Steffen et al., 2002; Brooks et al., 2006; Cobbett et al., 2007; Steen et al., 2009), and not through direct measurement of wet and dry deposition, making it difficult to evaluate the accuracy of models predictions. To the best of our knowledge, NYA is the only site out of the four Arctic sites where wet deposition measurements have been reported (Sprovieri et al.,

2016a). From May to December 2013, the observed net wet deposition flux is equal to 0.9 µg m^{-2} while modeled fluxes amount to 1.7, 3.2, 2.8, and 2.4 µg m^{-2} according to GLEMOS, GEOS-Chem, GEM-MACH-Hg, and ECHMERIT, respectively. All four models overestimate the wet deposition flux. Interestingly, all four models also overestimate the amount of precipitation (by a factor of 2.0, 2.2, 2.1, and 1.1, respectively. Data not shown). Several studies showed that the form of precipitation (rain *vs.* snow) influences the collection efficiency of the sampler. Lynch et al. (2003) and Prestbo and Gay (2009) found that the annual collection efficiency is 89 % and 87.1 ± 6.5 %, respectively, at cold weather sites of the United States and Canada experiencing snowfall in winter *vs* 98.8 ± 4.3 % at warm weather sites (Prestbo and Gay, 2009). Assuming an annual 89 % collection efficiency of snow at NYA does not narrow the gap between observed and modeled amounts of precipitation. However, an annual 89 % collection efficiency at NYA seems generous considering that snow falls year round and that strong wind (> 10 m s^{-1}) and blowing snow are frequent, especially in winter (Maturilli et al., 2013).

3.2 Antarctic sites

3.2.1 Observations

Fig. 2b shows monthly box plots of all data collected in Antarctica (ground-based sites and cruises). Hg(0) concentrations from the ANT cruises displayed in Fig.2b refer to data collected when R/V Polarstern operated within the marginal sea ice region (from 8 July to 23 July 2013, from 25 July to 9 August 2013, and from 28 August to 5 October 2013) (Nerentorp Mastromonaco et al., 2016). Similarly, Hg(0) concentrations from the OSO cruise refer to data collected at latitude > 60°S. Hg(0) concentrations measured during the ANT and OSO cruises are somewhat higher than values at ground-based Antarctic sites. The average value at Antarctic sites is 0.96 ± 0.32 ng m^{-3}, i.e. 35 % lower than the average value at Arctic sites (see section 3.1). This result is consistent with the North-to-South Hg(0) decreasing gradient reported by Sprovieri et al. (2016b), and with values reported at Southern Hemisphere mid-latitudes sites (Angot et al., 2014; Slemr et al., 2015).

The Hg(0) concentration data from the three Antarctic ground-based sites for the period 2011-2015 are presented as monthly box and whisker plots in Fig. 9. Information regarding annually- and monthly-based statistics at the three sites can be found in Tables 2 and 3, respectively. The annual medians for 2011-2015 at TR and 2012-2015 at DDU (Table 2) suggest a low inter annual variability in the distribution of Hg(0) concentrations. Conversely,

Hg(0) concentrations are notably higher in 2015 than in 2012 and 2013 at DC. This trend is more apparent from Fig. 9b, especially from March to September. It is worth noting that in 2015 measurements were performed at a different location within the "clean area" (the instrument was moved from one shelter to another). Additionally, following the January 2014 instrument failure, a new Tekran instrument operated in 2015. The combination of these two elements likely, at least partly, explains the offset observed in 2015. Despite this offset, the seasonal trends of Hg(0) repeat from year to year at DC (see below).

The mean seasonal variation of Hg(0) concentrations at Antarctic ground-based sites is displayed in Fig. 4b. Summer refers to November-February, fall to March-April, winter to May-August, and spring to September-October. At TR, the Hg(0) concentrations are significantly (p value < 0.0001, Mann-Whitney test) higher in winter (0.98 ± 0.06 ng m^{-3}) than in summer (0.89 ± 0.29 ng m^{-3}), in good agreement with the seasonal variation reported at TR by Pfaffhuber et al. (2012) from February 2007 to June 2011, and at Neumayer (NM) by Ebinghaus et al. (2002). Contrarily, Hg(0) concentrations at DDU are slightly but significantly (p value < 0.0001, Mann-Whitney test) higher in summer (0.88 ± 0.32 ng m^{-3}) than in winter (0.84 ± 0.11 ng m^{-3}). On the high-altitude Antarctic plateau at DC, Hg(0) concentrations exhibit a distinct maximum in fall (1.45 ± 0.27 ng m^{-3}) and a minimum in summer (0.78 ± 0.46 ng m^{-3}). The mechanisms which cause the seasonal variation of Hg(0) concentrations at Antarctic sites are discussed in the following sections.

3.2.1.1 The winter mysteries

Hg(0) concentrations at TR remain at a fairly constant level of 0.98 ± 0.06 ng m^{-3} in average from April to August (Fig. 2b). This result is in good agreement with observations at Neumayer (Ebinghaus et al., 2002). Pfaffhuber et al. (2012) attributed this phenomenon to the lack of photochemical oxidation processes during the polar night. Conversely, Hg(0) concentrations exhibit a gradual 30 % decrease at DC, from 1.48 ± 0.19 in average in April to 0.98 ± 0.20 ng m^{-3} in August. This decreasing trend remains unexplained and possibly results from the dry deposition of Hg(0) onto the snowpack (Angot et al., 2016b). In 2013, measurements were performed at various height levels above the snow surface. Interestingly, Angot et al. (2016b) reported a steeper decrease of Hg(0) concentrations close to the snow surface suggesting that the snowpack may act as a sink for mercury. Similarly, a gradual 20 % decrease in Hg(0) concentrations is observed at DDU, from 0.94 ± 0.07 in average in April to 0.72 ± 0.10 ng m^{-3} in August (Fig. 2b). Based on an analysis of air mass back trajectories, Angot et al. (2016a) suggested that this decreasing trend at DDU most likely results from

reactions occurring within the shallow boundary layer on the Antarctic plateau, subsequently transported toward the coastal margins by katabatic winds. DDU is most of the time influenced by inland air masses whereas several studies showed that stations such as NM are not significantly impacted by air masses originating from the Antarctic plateau (Helmig et al., 2007; Legrand et al., 2016b) explaining why concentrations remain rather stable at NM and TR throughout winter.

Hg(0) concentration exhibits abrupt increases when moist and warm air masses from lower latitudes occasionally reach the three ground-based Antarctic stations. At DDU, such events are concomitant with an enhanced fraction of oceanic air masses reaching the site according to the HYSPLIT model simulations, and with increased sodium concentrations (Angot et al., 2016a). At DC, these advections of warm and moist air masses are confirmed by an increase of temperature at 10 m a.g.l. and a high integrated water vapor column (Angot et al., 2016b). Finally, based on a statistical analysis of source and sink regions, Pfaffhuber et al. (2012) showed that transport from lower-latitude regions are frequently associated with the highest Hg(0) concentrations at TR.

During the winter expedition ANTXXIX/6 on board R/V Polarstern over the Weddell Sea (Fig. 1), Nerentorp Mastromonaco et al. (2016) observed depletions of Hg(0) characterized by strong correlations with O_3. This is the first evidence of Hg(0) depletions occurring in winter. The authors propose a dark mechanism involving Br_2. AMDEs in Antarctica are operationally defined as Hg(0) concentrations below 0.60 ng m^{-3} (Pfaffhuber et al., 2012). Based on this threshold and on the O_3 signal, there is no evidence of Hg(0) depletions occurring during months of complete darkness at the three ground-based Antarctic sites.

3.2.1.2 Springtime AMDEs

Before going further, it should be noted that TR is not a coastal station. It is located at an elevation of 1275 m and approximately 220 km from the Antarctic coast. Contrarily, DDU is located on a small island about one km offshore from the Antarctic mainland.

AMDEs are observed at TR in positive correlation with O_3 (r up to 0.56, p value < 0.001, Spearman test). Based on the 0.60 ng m^{-3} threshold (see previous section), AMDEs occur in 2 % of the springtime observations, in line with the occurrence frequency of 5 % reported by Pfaffhuber et al. (2012) from February 2007 to June 2011. Based on a statistical analysis of source and sink regions, Pfaffhuber et al. (2012) indicated that the spring Hg(0) sink, caused by AMDEs, is mainly located within sea ice dense areas surrounding Queen Maud Land.

AMDEs at TR are weaker and less frequent when compared to the Arctic (see section 3.1.1.2) likely partly due to the location of the station not being exposed directly to depletion events but rather to transport of mercury-depleted air masses (Pfaffhuber et al., 2012). In contrast, AMDEs occur in 28 % of the observations from 28 August to 5 October 2013 during the spring expedition ANTXXIX/7 over sea ice areas of the Weddell Sea. At DDU, on the other side of the Antarctic continent, data covering the spring period are scarce (Table 3). As indicated by Angot et al. (2016a), the absence of depletions in spring 2012 tends to suggest that AMDEs, if any, are not very frequent at DDU. Several studies reported a less efficient bromine chemistry in East compared to West Antarctica due to a less sea-ice coverage (Theys et al., 2011; Legrand et al., 2016a). However, Angot et al. (2016a) reported low Hg(0) concentrations (0.71 ± 0.11 ng m^{-3}) and a significant positive correlation with O_3 (r up to 0.65, *p* value < 0.0001, Spearman test) in springtime oceanic air masses, likely due to bromine chemistry.

3.2.1.3 Boundary layer dynamics on the Antarctic plateau in fall

The fall maximum at DC likely partly results from a low boundary layer oxidative capacity under low solar radiation limiting Hg(0) oxidation. Additionally, at DC, weak turbulence and mixing, and strong temperature gradients near the surface are favored by light wind and clear sky conditions (Argentini et al., 2013). The surface-based temperature inversions were characterized by Pietroni et al. (2012) over the course of a year. In summer, a convective boundary layer characterized by a maximum depth of 200-400 m (Argentini et al., 2005) develops around midday. In winter, strong temperature inversions allow for a mixing depth of a few tens of meters only. Based on the limited area model MAR (Modèle Atmosphérique Régional), Angot et al. (2016b) indicated that the fall distinct maximum of Hg(0) concentrations is concomitant with the time when the boundary layer lowers to ~ 50 m in average and no longer exhibits a pronounced diurnal cycle. Hg(0) is thus suddenly dispersed into a reduced volume of air, limiting the dilution. Similarly, several studies showed that NO_x mixing ratios are enhanced when the boundary layer is shallow (Neff et al., 2008; Frey et al., 2013).

3.2.1.4 Extremely active processes in summertime

Summertime Hg(0) concentrations at the three ground-based sites exhibit a high variability (Fig. 2b), suggesting extremely active processes at this time of the year. Undetected from March to October, a diurnal cycle characterized by a noon Hg(0) maximum is observed in summer at DDU and DC over the 2012-2015 period (Angot et al., 2016a; Angot et al.,

2016b). At DC (DDU), Hg(0) concentrations range from ~ 0.6 ng m^{-3} (~ 0.7 ng m^{-3}) on average at night to ~ 1.0 ng m^{-3} (~ 1.1 ng m^{-3}) on average around midday. Conversely, there is no diurnal variation in Hg(0) concentrations at TR, in good agreement with observations reported by Pfaffhuber et al. (2012) from February 2007 to June 2011. Similarly, there is no mention of a daily cycle at NM, Terra Nova Bay, and McMurdo where summer campaigns were carried out (Ebinghaus et al., 2002; Temme et al., 2003; Sprovieri et al., 2002; Brooks et al., 2008b). The absence of diurnal cycle at TR can be attributed to the absence of sources/sinks for Hg(0) with a diurnal cycle in the vicinity of the site (Pfaffhuber et al., 2012). The mean summertime Hg(0) concentration is significantly (p value < 0.0001, Mann-Whitney test) lower at DC (0.78 ± 0.46 ng m^{-3}) than at DDU (0.88 ± 0.32 ng m^{-3}) and TR (0.89 ± 0.29 ng m^{-3}), suggesting a more intense oxidation of Hg(0). The boundary layer oxidative capacity has been shown to be high in summer on the Antarctic plateau with elevated levels of OH, O_3, NO_x, and RO_2 radicals (Davis et al., 2001; Grannas et al., 2007; Eisele et al., 2008; Kukui et al., 2014; Frey et al., 2015). Angot et al. (2016b) performed Hg(0) measurements in both the atmospheric boundary layer and the interstitial air of the snowpack, and analyzed total mercury in surface snow samples. The authors, in good agreement with Brooks et al. (2008a) and Dommergue et al. (2012), suggested that the observed summertime Hg(0) diurnal cycle at DC might be due to a dynamic daily cycle of Hg(0) oxidation, deposition to the snowpack, and reemission from the snowpack. Similarly, a recent study (Wang et al., 2016) reported a Hg(0) diurnal cycle at Kunlun station (80°25'S, 77°6'E) located near Dome A (80°22'S, 77°27'E) – the highest elevation point on the Antarctic plateau (4090 m). This suggests that the dynamic daily cycle of Hg(0) oxidation, deposition to the snowpack, and reemission from the snowpack probably occurs throughout the Antarctic plateau. Based on an analysis of air mass back trajectories, Angot et al. (2016a) showed that measurements at DDU on the East Antarctic coast are dramatically influenced by air masses exported from the Antarctic Plateau by strong katabatic winds. The advection of inland air masses enriched in oxidants – NO_x, O_3, and OH (Grilli et al., 2013; Kukui et al., 2012) – and Hg(II) species likely results in the build-up of an atmospheric reservoir of Hg(II) species at DDU, as supported by elevated levels of total mercury in surface snow samples (Angot et al., 2016a). The diurnal cycle observed at DDU – regardless of wind speed and direction – might result from a local dynamic cycle of oxidation/deposition/reemission in the presence of elevated levels of Hg(II) species along with emissions of mercury from ornithogenic soils – formed by an accumulation of penguin excreta.

Hg(0) depletion events occur each year in summer at DC with Hg(0) concentrations remaining low (~ 0.40 ng m^{-3}) for several weeks. These depletion events do not resemble to the ones observed in the Arctic. They are not associated with depletions of O_3, and occur as air masses stagnate over the Plateau which could favor an accumulation of oxidants within the shallow boundary layer (Angot et al., 2016b). At TR, Pfaffhuber et al. (2012) reported episodic low Hg(0) concentrations in summer, anti-correlated with O_3, and associated with the transport of inland air masses. Results at TR (Pfaffhuber et al., 2012) and DDU (Angot et al., 2016a), along with observations from earlier studies at other coastal Antarctic sites (Sprovieri et al., 2002; Temme et al., 2003), demonstrate that the inland atmospheric reservoir can influence the cycle of atmospheric mercury at a continental scale, especially in areas influenced by recurrent katabatic winds.

Additionally, Pfaffhuber et al. (2012) indicated that the ocean is a source of mercury to TR. Similarly, at DDU, Angot et al. (2016a) reported elevated (1.04 ± 0.29 ng m^{-3}) Hg(0) concentrations in oceanic air masses along with a significant positive correlation between Hg(0) and the daily-averaged percentage of oceanic air masses ($r = 0.50$, p value < 0.0001, Spearman test). These results are in line with the summer Hg(0) enhancement in the Arctic likely partly due to oceanic evasion from ice-free open waters (see section 3.1.1.3).

3.2.2 Comparison with models

Table 4 displays goodness-of-fit statistics between monthly-averaged modeled and observed data in 2013. ECHMERIT slightly underestimates Hg(0) concentrations at the three ground-based Antarctic sites. Contrarily, the three other global models overestimate Hg(0) levels, suggesting an underestimation of sinks. The ability of the four models to reproduce the observed seasonality of Hg(0) concentrations at ground-based Antarctic sites in 2013 is shown in Fig. 6b and discussed in the following sections. The inter-annual variability of the monthly Hg(0) concentration distribution at Antarctic ground-based sites as simulated by GEM-MACH-Hg and GEOS-Chem is displayed in Fig. 7b while Table 5 shows the percent bias between hourly-averaged modeled and observed data on a seasonal basis from 2011 to 2014.

3.2.2.1 Seasonal variation

a) Winter

GEOS-Chem, GEM-MACH-Hg, and GLEMOS overestimate year 2013 Hg(0) concentrations in winter at the three ground-based stations (Fig. 6a). This trend repeats year after year for

GEOS-Chem and GEM-MACH-Hg (Table 5). The most striking result, however, is the modeled gradual increase of Hg(0) concentrations over the course of winter at the three ground-based sites according to ECHMERIT, GEOS-Chem, and GEM-MACH-Hg. A mean gradual increase of 9 %, 19 %, and 11 % is predicted by the three models, respectively, from May to August. GLEMOS, however, predicts a mean gradual decrease of 5 % over the course of winter at the three sites. It is to be noted (see section 3.2.1.1) that Hg(0) concentrations are constant from May to August at TR, exhibit a gradual 30 % decrease at DC possibly due to the dry deposition of Hg(0), and a gradual 20 % decrease at DDU due to advection of inland air masses. All in all, the four models misrepresent the decreasing trend at DC and DDU. This might be due to several factors including underestimation of concentrations of oxidants over the East Antarctic plateau at this period of the year, omission of heterogeneous mechanisms, and significant bias in Southern Hemisphere emissions, including oceanic evasion. The strong increase (19 %) of Hg(0) concentrations from May to August predicted by GEOS-Chem is not restricted to the Antarctic continent but is obtained for the whole Southern Hemisphere (Fig. 3 in Song et al., 2015). The emission inversion performed by Song et al. (2015) overturns the seasonality of oceanic emissions and better reproduces the ground-based Hg(0) observations in the Southern Hemisphere mid-latitudes and at TR. Further work, including sensitivity tests, is needed to explain the discrepancies between observed and modeled trends.

Additionally, all of the four models are unable to capture the differences in trends observed at the three ground-based sites (constant *vs.* decreasing concentrations). As discussed in section 3.2.1.1, TR, contrarily to DDU, is not significantly influenced by inland air masses. This large-scale airflow pattern will have to be captured by models in order to better reproduce observations. Interestingly, Zatko et al. (2016) calculated the annual mean surface wind convergence/divergence over the Antarctic continent using GEOS-Chem. The results – consistent with those by Parish and Bromwich (1987) and Parish and Bromwich (2007) – correctly indicate that the large-scale airflow pattern in Antarctica flows from the East Antarctic plateau towards the coastal margins and accurately highlight major regions of wind convergence. The findings from this study can be used as the basis for future research.

b) Spring

Based on the 0.60 ng m^{-3} threshold, GEM-MACH-Hg and GEOS-Chem do not predict any AMDE at TR over the 2011-2014 period. Considering the low occurrence frequency based on observations (2 %, see section 3.2.1.2), this result is not unreasonable. Similarly, GEM-MACH-Hg does not predict any AMDE at DDU. However, GEOS-Chem predicts AMDEs in

1.5 % of the springtime observations at DDU. This over-prediction of AMDEs at DDU likely results from the constant value of 5 pptv of BrO added in the springtime Antarctic boundary layer. While Saiz-Lopez et al. (2007) reported a spring maximum of up to 7 pptv at Halley Station (75°35'S, 26°30'W, West Antarctic coast), Legrand et al. (2016a) suggested a BrO mixing ratio ≤ 1 pptv at DDU (East Antarctic coast) in spring using an off-line chemistry transport model. Based on the oxygen and nitrogen isotope analysis of airborne nitrate, Savarino et al. (2007) provided further evidence for low BrO levels in the vicinity of DDU.

c) Fall

None of the four models capture the fall maximum at DC (Fig. 6b). While a spatially and temporally resolved distribution of concentrations of oxidants on the East Antarctic Plateau is needed, the boundary layer dynamics must also be taken into account. Based on the work by Lin and McElroy (2010), Zatko et al. (2016) incorporated a calculation of the boundary layer height across Antarctica and Greenland into GEOS-Chem. One could also rely on model outputs from the limited area model MAR, validated against observations at DC (Gallée and Gorodetskaya, 2010; Gallée et al., 2015). This model agrees very well with observations and provides reliable and useful information about surface turbulent fluxes, vertical profiles of vertical diffusion coefficients and boundary layer height.

d) Summer

The daily variation of Hg(0) concentrations was investigated based on hourly-averaged data provided by GEOS-Chem and GEM-MACH-Hg. The two models are not able to reproduce the noon maximum observed at DC and DDU in summer (3.2.1.4), suggesting that the dynamic daily cycle of deposition and reemission at the air/snow interface is not captured by the models. The bidirectional exchange of Hg(0) is complex and influenced by multiple environmental variables (e.g., UV intensity, temperature, atmospheric turbulence, presence of reactants) limiting the accuracy of flux modeling (Zhu et al., 2016). The work carried out by Durnford et al. (2012) in the Arctic and by Zatko et al. (2016) in Antarctica could be good starting points for future research. The former developed a new dynamic physically-based snowpack model to determine the fate of mercury deposited onto snowpacks; the latter incorporated an idealized snowpack along with a snow radiative transfer model (Zatko et al., 2013) into GEOS-Chem to investigate the impact of snow nitrate photolysis on the boundary layer chemistry across Antarctica.

3.2.2.2 Reactive mercury and deposition

According to Fig. 8b, ECHMERIT predicts low RM concentrations during the whole 2013 year at the three ground-based stations (annual averages of 10, 7, and 6 pg m^{-3} at TR, DC, and DDU, respectively). GEOS-Chem predicts a peak in spring at the three sites (up to ~ 160 pg m^{-3} in average October at DC), and quite elevated concentrations in summer and fall (~ 85 pg m^{-3} in average). GEM-MACH-Hg predicts increased concentrations in summer at TR and DDU only. Finally, GLEMOS predicts a more intense summer peak at DC (up to ~ 130 pg m^{-3} in average in November) than at DDU and TR. Measurements of RM are scarce in Antarctica and have never been reported on a year-round basis. RM concentrations ranging from 100 to 1000 pg m^{-3} have been reported in summer at South Pole (Brooks et al., 2008a) and several studies have reported elevated concentrations at coastal sites in spring during the AMDEs season (165 pg m^{-3} in average at Mc Murdo (Brooks et al., 2008b)) and in summer (mean RGM concentration of 116 pg m^{-3} at Terra Nova Bay (Sprovieri et al., 2002); RGM and Hg(p) concentrations ranging from 5 to > 300 pg m^{-3} and from 15 to 120 pg m^{-3}, respectively, at Neumayer (Temme et al., 2003)). These results along with the seasonal pattern of Hg(0) reported in section 3.2.1 suggest that the atmospheric boundary layer is enriched in RM in summer, especially on the Antarctic plateau, and that the four models tend to underestimate the summertime concentrations. Year-round measurements are needed to further evaluate the accuracy of models predictions.

The total (wet + dry) deposition flux for year 2013 is equal to 1.0, 3.3, 2.5, and 3.9 µg m^{-2} yr^{-1} at TR, 0.8, 1.5, 0.8, and 1.1 µg m^{-2} yr^{-1} at DC, and 4.3, 9.7, 9.7, and 4.1 µg m^{-2} yr^{-1} at DDU according to GLEMOS, GEOS-Chem, GEM-MACH-Hg, and ECHMERIT, respectively. Deposition during summertime accounts for 73, 53, 68, and 35 % of the total deposition at TR, 58, 50, 37, and 35 % at DC, and 58, 61, 89, and 28 % at DDU according to GLEMOS, GEOS-Chem, GEM-MACH-Hg, and ECHMERIT, respectively. There are no measurements of wet and dry deposition in Antarctica, except Angot et al. (2016b) who reported a Hg(0) dry deposition velocity of 9.3 10^{-5} cm s^{-1} in winter at DC. Similarly to the Arctic (see section 3.1.2.2), deposition of mercury is typically inferred from concentrations of total mercury in the snowpack. To the best of our knowledge, results found in Angot et al. (2016b) are the only reported over various seasons. Higher total mercury concentrations in surface snow samples in summer suggest an enhanced deposition at this period of the year. Alternatively, deposition of mercury can be inferred from the biomonitoring of Antarctic macrolichens and mosses (Bargagli, 2016). Large-scale and long-term biomonitoring surveys of mercury deposition have been performed in Victoria Land (Bargagli et al., 1993; Bargagli et al., 2005). While all

four models predict higher total mercury deposition for year 2013 at high Arctic (ALT, SND, NYA) *vs.* Antarctic ground-based sites, significantly higher mercury concentrations in Antarctic *vs.* Northern Hemisphere lichens suggest otherwise (Bargagli et al., 1993).

Wet deposition accounts for 14, 53, 47, and 0 % of the total (wet + dry) flux at TR, 35, 7, 14, and 0 % at DC, and 68, 57, 60, and 8 % at DDU according to GLEMOS, GEOS-Chem, GEM-MACH-Hg, and ECHMERIT, respectively. The amount of precipitation is equal to 214, 242, 291, and 1127 mm yr^{-1} at TR, 33, 29, 24, and 60 mm yr^{-1} at DC, and 643, 792, 895, and 1751 mm yr^{-1} at DDU according to GLEMOS, GEOS-Chem, GEM-MACH-Hg, and ECHMERIT, respectively. Ground-based measurements of precipitation are sparse and difficult to obtain in Antarctica. Strong winds in coastal regions make it difficult to tell the difference between blowing snow and precipitation (Palerme et al., 2014). On the Antarctic plateau, a significant part of the precipitation falls in the form of ice crystals (diamond dust) under clear-sky conditions (Bromwich, 1988; Fujita and Abe, 2006). Satellite observations of precipitation in Antarctica by active sensors are now possible (Liu, 2008; Stephens et al., 2008). According to Palerme et al. (2014), the mean annual snowfall rate is < 20 mm water equivalent yr^{-1} at DC, ranges from 20 to 100 mm yr^{-1} at TR, and from 500 to 700 mm yr^{-1} at DDU. The low amount of precipitation at DC might, however, be offset by the high mercury-capture efficiency of ice crystals (Douglas et al., 2008) that are frequently observed at that site (Bromwich, 1988; Fujita and Abe, 2006).

4 Summary and future perspectives

The data compiled in this study represent the latest available in Polar Regions. While the Arctic is a semi-enclosed ocean almost completely surrounded by land, Antarctica is a land mass – covered with an immense ice shelf – surrounded by ocean. Therefore, the cycle of atmospheric mercury in the two regions presents both similarities and differences. Springtime AMDEs are observed in both regions at coastal sites (see sections 3.1.1.2 and 3.2.1.2). Their frequency and magnitude depend on parameters such as sea-ice dynamics, temperature, and concentration of bromine species, and exhibit a significant but poorly understood inter-annual variability. Additionally, coastal sites in the two regions are influenced by both snowpack reemission and oceanic evasion of Hg(0) in summer (see sections 3.1.1.3 and 3.2.1.4). As evidenced in section 3.1.1.3, the summertime enhancement of Hg(0) concentrations exhibits a significant but little understood inter-annual variability at Arctic sites. The cycle of atmospheric mercury differs between the Arctic and Antarctica, primarily because of their

different geography. Arctic sites are significantly influenced by mercury emissions from Northern Hemisphere mid-latitudes – especially in winter (see section 3.1.1.1). Coastal Antarctic sites are significantly influenced by the reactivity of atmospheric mercury observed on the Antarctic Plateau due to the large-scale airflow pattern flowing from the East Antarctic ice sheet towards the coastal margins (katabatic winds). As discussed in section 3.2, the cycle of atmospheric mercury on the Antarctic Plateau is surprising and involves yet unraveled mechanisms in winter and a daily bidirectional exchange of Hg(0) at the air/snow interface in summer.

From the comparison of multi-model simulations with observations, we identified whether the processes that affect Hg(0) seasonality and inter-annual variability, including mercury oxidation, deposition and reemission, are appropriately understood and represented in the models. Generally, models reproduce quite fairly the observed seasonality at Arctic sites but fail to reproduce it at Antarctic sites. In order for the models to reproduce the seasonality of Hg(0) concentrations in Antarctica, parameterization of the boundary layer dynamics (see section 3.1.1.3) and of the large-scale airflow pattern (see above) is needed. Moreover, reaction pathways might be missing or inappropriately incorporated in models. Heterogeneous reactions, although poorly understood (Subir et al., 2012), might be required to explain the reactivity on the Antarctic Plateau. Additionally, while NO_x chemistry was shown to prevail upon halogens chemistry in East Antarctica in summer (Legrand et al., 2009; Grilli et al., 2013) it is currently incorporated in none of the four global models.

Based on this study, the following research gaps need to be addressed:

1. Improving the spatial resolution of RM measurements. There is presently no year-round data available in Antarctica. The Tekran speciation unit suffers from significant biases and interferences, is expensive, labor-intensive, and requires trained operators. Passive samplers, such as Polyethersulfone cation exchange membranes, could provide an alternative (Huang et al., 2014) but further tests are needed to assess their collection efficiency and potential biases.

2. Unraveling of Hg(II) speciation. The exact speciation – expected to vary with space and time – remains unknown. Identification of Hg(II) species in ambient air emerges as one of the priorities for future research (Gustin et al., 2015). Recent advancement on analytical techniques may offer new insights into Hg(II) speciation (Huang et al., 2013; Jones et al., 2016) but further research is still needed. Such advancement will greatly improve our understanding of atmospheric redox processes.

3. Improving the spatial resolution of measurements of total mercury in snow samples. These measurements are an alternative to wet and dry deposition measurements – difficult to perform in Polar Regions.

4. Investigation of the fundamental environmental processes driving the inter-annual variability of Hg(0) concentrations, especially at Arctic sites. Further work is needed to establish the degree to which temperature and sea-ice dynamics across the Arctic alters mercury chemistry in spring and summer. This will also open up new opportunities to explore the influence of Climate Change on the cycle of mercury in Polar Regions.

5. Investigation (and quantification) of the oceanic fluxes of Hg(0) during oceanographic campaigns across the Arctic and Austral Oceans. This will largely reduce the uncertainty in the mercury budget estimation in Polar Regions.

6. Reducing uncertainties in existing kinetic parameters and quantitatively investigate the effect of temperature on the rate constants (Subir et al., 2011). Limited data are available for temperature applicable to atmospheric conditions, especially in Polar Regions. Achieving this will largely reduce uncertainties in atmospheric models.

7. Investigation of the influence of atmospheric surfaces (e.g., aerosols, clouds, ice, snow covers, ice crystals). This is a major gap for adequate modeling of mercury cycling (Subir et al., 2012) and studies addressing this are critically needed.

Acknowledgements

HA, OM, and AD thank the overwintering crew: S. Aguado, D. Buiron, N. Coillard, G. Dufresnes, J. Guilhermet, B. Jourdain, B. Laulier, S. Oros, A. Thollot, and N. Vogel at DDU, S. Aubin, A. Barbero, N. Hueber, C. Lenormant, and R. Jacob at DC. This work contributed to the EU-FP7 project Global Mercury Observation System (GMOS, www.gmos.eu) and has been supported by a grant from Labex OSUG@2020 (Investissements d'avenir – ANR10 LABX56), and the Institut Universitaire de France. Logistical and financial support was provided by the French Polar Institute IPEV (Program 1028, GMOstral). KAP thanks the Norwegian Environmental Agency and the Norwegian Antarctic Research Expeditions for long-term financial support of Norwegian mercury measurements and in particular the technicians J.H. Wasseng and A. Bäcklund at NILU for their excellent care taking of the Tekran monitors. NES and SS acknowledge support from the U.S. National Science Foundation Atmospheric Chemistry Program under grant #1053648.

References

ECMWF: European Centre for Medium-Range Weather Forecasts. http://www.ecmwf.int/en/forecasts/datasets, access: 20 January 2016.

Adams, J. W., Holmes, N. S., and Crowley, J. N.: Uptake and reaction of HOBr on frozen and dry NaCl/NaBr surfaces between 253 and 233 K, Atmos. Chem. Phys., 2, 79-91, 10.5194/acp-2-79-2002, 2002.

AMAP: Human Health in the Arctic. Arctic Monitoring and Assessment Programme (AMAP), Oslo, Norway, 165pp, 2015.

Amos, H. M., Jacob, D. J., Holmes, C. D., Fisher, J. A., Wang, Q., Yantosca, R. M., Corbitt, E. S., Galarneau, E., Rutter, A. P., Gustin, M. S., Steffen, A., Schauer, J. J., Graydon, J. A., St. Louis, V. L., Talbot, R. W., Edgerton, E. S., Zhang, Y., and Sunderland, E. M.: Gas-particle partitioning of atmopheric Hg(II) and its effect on global mercury deposition, Atmospheric Chemistry and Physics, 12, 591-603, 2012.

Amos, H. M., Sonke, J. E., Obrist, D., Robins, N., Hagan, N., Horowitz, H. M., Mason, R. P., Witt, M. L. I., Hedgecock, I. M., Corbitt, E. S., and Sunderland, E. M.: Observational and modeling constraints on global anthropogenic enrichment of mercury, Environmental Science and Technology, 49, 4036-4047, 2015.

Andersson, M. E. S., J., Gårdfeldt, K., and Linfqvist, O.: Enhanced concentrations of dissolved gaseous mercury in the surface waters of the Arctic Ocean, Marine Chemistry, 110, 190-194, 2008.

Angot, H., Barret, M., Magand, O., Ramonet, M., and Dommergue, A.: A 2-year record of atmospheric mercury species at a background Southern Hemisphere station on Amsterdam Island, Atmospheric Chemistry and Physics 14, 11461-11473, 2014.

Angot, H., Dion, I., Vogel, N., Magand, O., Legrand, M., and Dommergue, A.: Atmospheric mercury record at Dumont d'Urville, East Antarctic coast: continental outflow and oceanic influences, Atmospheric Chemistry and Physics Discussions, 10.5194/acp-2016-257, in review, 2016a.

Angot, H., Magand, O., Helmig, D., Ricaud, P., Quennehen, B., Gallée, H., Del Guasta, M., Sprovieri, F., Pirrone, N., Savarino, J., and Dommergue, A.: New insights into the atmospheric mercury cycling in Central Antarctica and implications at a continental scale, Atmospheric Chemistry and Physics Discussions, 10.5194/acp-2016-144, in review, 2016b.

Argentini, S., Viola, A., Sempreviva, A. M., and Petenko, I.: Summer boundary-layer height at the plateau site of Dome C, Antarctica, Boundary-Layer Meteorology, 115, 409-422, 2005.

Argentini, S., Petenko, I., Viola, A., Mastrantonio, G., Pietroni, I., Casasanta, G., Aristidi, E., and Ghenton, C.: The surface layer observed by a high-resolution sodar at Dome C, Antarctica, Annals of geophysics, 56, doi:10.4401/ag-6347, 2013.

Ariya, P. A., Dastoor, A. P., Amyot, M., Schroeder, W. H., Barrie, L., Anlauf, K., Raofie, F., Ryzhkov, A., Davignon, D., Lalonde, J., and Steffen, A.: The arctic: a sink for mercury, Tellus, 56B, 397-403, 2004.

Aspmo, K., Gauchard, P.-A., Steffen, A., Temme, C., Berg, T., Bahlmann, E., Banic, C., Dommergue, A., Ebinghaus, R., Ferrari, C., Pirrone, N., Sprovieri, F., and Wibetoe, G.: Measurements of atmospheric mercury species during an international study of mercury depletion events at Ny-Ålesund, Svalbard, spring 2003. How reproductible are our present methods?, Atmospheric Environment, 39, 7607-7619, 2005.

Aspmo, K., Temme, C., Berg, T., Ferrari, C., Gauchard, P.-A., Faïn, X., and Wibetoe, G.: Mercury in the atmosphere, snow and melt water ponds in the north atlantic ocean during Arctic summer, Environmental Science and Technology, 40, 4083-4089, 2006.

Balabanov, N. B., Shepler, B. C., and Peterson, K. A.: Accurate Global Potential Energy Surface and Reaction Dynamics for the Ground State of HgBr2, The Journal of Physical Chemistry A, 109, 8765-8773, 10.1021/jp053415l, 2005.

Bargagli, R., Battisti, E., Focardi, S., and Formichi, P.: Preliminary data on environmental distribution of mercury in northern Victoria Land, Antarctica, Antarctic Science, 5, 3-8, 1993.

Bargagli, R., Agnorelli, C., Borghini, F., and Monaci, F.: Enhanced deposition and bioaccumulation of mercury in antarctic terrestrial ecosystems facing a coastal polynya, Environmental Science and Technology, 39, 8150-8155, 2005.

Bargagli, R.: Moss and lichen biomonitoring of atmospheric mercury: a review, Science of the Total Environment, 572, 216-231, 2016.

Barrie, L. A., Hoff, R. M., and Daggupaty, S. M.: Arctic Air Chemistry Proceedings of the Second SymposiumThe influence of mid-latitudinal pollution sources on haze in the Canadian arctic, Atmospheric Environment (1967), 15, 1407-1419, http://dx.doi.org/10.1016/0004-6981(81)90347-4, 1981.

Berg, T., Bartnicki, J., Munthe, J., Lattila, H., Hrehoruk, J., and Mazur, A.: Atmospheric mercury species in the European Arctic: measurements and modelling, Atmospheric Environment, 35, 2569-2582, 2001.

Berg, T., Sekkesæter, S., Steinnes, E., Valdal, A.-K., and Wibetoe, G.: Springtime depletion of mercury in the European Arctic as observed at Svalbard, Science of The Total Environment, 304, 43-51, http://dx.doi.org/10.1016/S0048-9697(02)00555-7, 2003a.

Berg, T., Sommar, J., Wängberg, Gardfeldt, K., Munthe, J., and Schroeder, B.: Arctic mercury depletion events at two elevations as observed at the Zeppelin Station and Dirigibile Italia, Ny-Ålesund, spring 2002, J. Phys. IV France, 107, 151-154, 2003b.

Berg, T., Aspmo, K., and Steinnes, E.: Transport of Hg from atmospheric mercury depletion events to the mainland of Norway and its possible influence on Hg deposition, Geophysical research letters, 35, doi:10.1029/2008GL033586, 2008.

Berg, T., Pfaffhuber, K. A., Cole, A. S., Engelsen, O., and Steffen, A.: Ten-year trends in atmospheric mercury concentrations, meteorological effects and climate variables at Zeppelin, Ny-Alesund, Atmospheric Chemistry and Physics, 13, 6575-6586, 2013.

Bey, I., Jacob, D. J., Yantosca, R. M., Logan, J. A., Field, B. D., Fiore, A. M., li, Q., Liu, H. Y., Mickley, L. J., and Schultz, M. G.: Global modeling of tropospheric chemistry with assimilated meteorology: model description and evaluation, Journal of geophysical research, 106, 23,073-023,095, 2001.

Bilello, M. A.: Prevailing wind directions in the Arctic Ocean, Corps of Engineers, U. S. Army: Hanover, New Hampshire, 38, 1973.

Bloom, N. S., and Fitzgerald, W. F.: Determination of volatile mercury species at the picogram level by low temperature gas chromatography with cold-vapor atomic fluorescence detection, Analytica Chimica Acta, 208, 151-161, 1988.

Bourgeois, Q., and Bey, I.: Pollution transport efficiency toward the Arctic: senstivity to aerosol scavenging and source regions, Journal of geophysical research, 116, 10.1029/2010JD015096, 2011.

1074 Bromwich, D. H.: Snowfall in high southern latitudes, Rev. Geophys., 26, 149-168,
1075 http://dx.doi.org/10.1029/RG026i001p00149, 1988.

1076 Brooks, S., Saiz-Lopez, A., Skov, H., Lindberg, S. E., Plane, J. M. C., and Goodsite, M. E.:
1077 The mass balance of mercury in the springtime arctic environment, Geophysical research
1078 letters, doi: 10.1029/2005GL025525, 2006.

1079 Brooks, S. B., Arimoto, R., Lindberg, S. E., and Southworth, G.: Antarctic polar plateau snow
1080 surface conversion of deposited oxidized mercury to gaseous elemental mercury with
1081 fractional long-term burial, Atmospheric Environment, 42, 2877-2884, 2008a.

1082 Brooks, S. B., Lindberg, S. E., Southworth, G., and Arimoto, R.: Springtime atmospheric
1083 mercury speciation in the McMurdo, Antarctica coastal region, Atmospheric Environment,
1084 42, 2885-2893, 2008b.

1085 Cadle, S. H.: Dry Deposition to Snowpacks, in: Seasonal Snowpacks: Processes of
1086 Compositional Change, edited by: Davies, T. D., Tranter, M., and Jones, H. G., Springer
1087 Berlin Heidelberg, Berlin, Heidelberg, 21-66, 1991.

1088 Chen, L., Zhang, Y., Jacob, D. J., Soerensen, A. L., Fisher, J. A., Horowitz, H. M., Corbitt, E.
1089 S., and Wang, X.: A decline in Arctic Ocean mercury suggested by differences in decadal
1090 trends of atmospheric mercury between the Arctic and northern midlatitudes, Geophysical
1091 research letters, 42, 10.1002/2015GL064051, 2015.

1092 Cobbett, F. D., Steffen, A., Lawson, G., and Van Heyst, B. J.: GEM fluxes and atmospheric
1093 mercury concentrations (GEM, RGM and Hg(p)) in the Canadian Arctic at Alert, Nunavut,
1094 Canada (February–June 2005), Atmospheric Environment, 41, 6527-6543,
1095 http://dx.doi.org/10.1016/j.atmosenv.2007.04.033, 2007.

1096 Cole, A. S., and Steffen, A.: Trends in long-term gaseous mercury observations in the Arctic
1097 and effects of temperature and other atmospheric conditions, Atmos. Chem. Phys., 10, 4661-
1098 4672, 10.5194/acp-10-4661-2010, 2010.

1099 Cole, A. S., Steffen, A., Pfaffhuber, K. A., Berg, T., Pilote, M., Poissant, L., Tordon, R., and
1100 Hung, H.: Ten-year trends of atmospheric mercury in the high Arctic compared to Canadian
1101 sub-Arctic and mid-latitudes sites, Atmospheric Chemistry and Physics, 13, 1535-1545, 2013.

1102 D'Amore, F., Bencardino, M., Cinnirella, S., Sprovieri, F., and Pirrone, N.: Data quality
1103 through a web-based QA/QC system: implementation for atmospheric mercury data from the
1104 Global Mercury Observation System, Environmental Science: Processes & Impacts, 17, 1482-
1105 1491, 2015.

1106 Dastoor, A., Ryzhkov, A., Durnford, D., Lehnherr, I., Steffen, A., and Morrison, H.:
1107 Atmospheric mercury in the Canadian Arctic. Part II: Insight from modeling, Science of The
1108 Total Environment, 509–510, 16-27, http://dx.doi.org/10.1016/j.scitotenv.2014.10.112, 2015.

1109 Dastoor, A. P., and Larocque, Y.: Global circulation of atmospheric mercury: a modelling
1110 study, Atmospheric Environment, 38, 147-161, 2004.

1111 Dastoor, A. P., Davignon, D., Theys, N., Van Roozendael, M., Steffen, A., and Ariya, P. A.:
1112 Modeling dynamic exchange of gaseous elemental mercury at polar sunrise, Environmental
1113 Science and Technology, 42, 5183-5188, 2008.

1114 Dastoor, A. P., and Durnford, D. A.: Arctic ocean: is it a sink or a source of atmospheric
1115 mercury?, Environmental Science and Technology, 48, 1707-1717, 2014.

1116 Davis, D., Nowak, J. B., Chen, G., Buhr, M., Arimoto, R., Hogan, A., Eisele, F., Mauldin, L.,
1117 Tanner, D., Shetter, R., Lefer, B., and McMurry, P.: Unexpected high levels of NO observed
1118 at South Pole, Geophysical research letters, 28, 3625-3628, 2001.

1119 De Simone, F., Gencarelli, C. N., Hedgecock, I. M., and Pirrone, N.: Global atmospheric
1120 cycle of mercury: a model study on the impact of oxidation mechanisms, Environmental
1121 Science and Pollution Research, 21, 4110-4123, 2014.

1122 De Simone, F., Gencarelli, C. N., Hedgecock, I. M., and Pirrone, N.: A Modeling Comparison
1123 of Mercury Deposition from current Anthropogenic Mercury Emission Inventories,
1124 Environmental Science & Technology, 10.1021/acs.est.6b00691, 2016.

1125 Dibble, T. S., Zelie, M. J., and Mao, H.: Thermodynamics of reactions of ClHg and BrHg
1126 radicals with atmospherically abundant free radicals, Atmospheric Chemistry and Physics, 12,
1127 10271-10279, 2012.

1128 Dommergue, A., Larose, C., Faïn, X., Clarisse, O., Foucher, D., Hintelmann, H., Schneider,
1129 D., and Ferrari, C. P.: Deposition of Mercury Species in the Ny-Ålesund Area (79°N) and
1130 Their Transfer during Snowmelt, Environmental Science & Technology, 44, 901-907,
1131 10.1021/es902579m, 2010a.

1132 Dommergue, A., Sprovieri, F., Pirrone, N., Ebinghaus, R., Brooks, S., Courteaud, J., and
1133 Ferrari, C. P.: Overview of mercury measurements in the antarctic troposphere, Atmospheric
1134 Chemistry and Physics, 10, 3309-3319, 2010b.

1135 Dommergue, A., Barret, M., Courteaud, J., Cristofanelli, P., Ferrari, C. P., and Gallée, H.:
1136 Dynamic recycling of gaseous elemental mercury in the boundary layer of the antarctic
1137 plateau, Atmospheric Chemistry and Physics, 12, 11027-11036, 2012.

1138 Donohoue, D. L., Bauer, D., Cossairt, B., and Hynes, A. J.: Temperature and pressure
1139 dependent rate coefficients for the reaction of Hg with Br and the reaction of Br with Br: a
1140 pulsed laser photolysis-pulsed laser induced fluorescence study, Journal of physical
1141 chemistry, 110, 6623-6632, 2006.

1142 Douglas, T. A., Sturm, M., Simpson, W. R., Blum, J. D., Alvarez-Aviles, L., Keeler, G. J.,
1143 Perovich, D. K., Biswas, A., and Johnson, K.: Influence of snow and ice crystal formation and
1144 accumulation on mercury deposition to the Arctic, Environmental Science and Technology,
1145 42, 1542-1551, 2008.

1146 Douglas, T. A., Loseto, L. L., Macdonald, R. W., Outridge, P. M., Dommergue, A., Poulain,
1147 A. J., Amyot, M., Barkay, T., Berg, T., Chételat, J., Constant, P., Evans, M. J., Ferrari, C.,
1148 Gantner, N., Johnson, M. S., Kirk, J., Kroer, N., Larose, C., Lean, D., Gissel Nielsen, T.,
1149 Poissant, L., Rognerud, S., Skov, H., Sørensen, S., Wang, F., Wilson, S., and Zdanowicz, C.:
1150 The fate of mercury in Arctic terrestrial and aquatic ecosystems, a review, Environ. Chem., 9,
1151 321-355, http://dx.doi.org/10.1071/EN11140, 2012.

1152 Driscoll, C. T., Mason, R. P., Chan, H. M., Jacob, D. J., and Pirrone, N.: Mercury as a global
1153 pollutant: sources, pathways, and effects, Environmental Science and Technology, 47, 4967-
1154 4983, 2013.

1155 Dumarey, R., Temmerman, E., Dams, R., and Hoste, J.: The accuracy of the vapour injection
1156 calibration method for the determination of mercury by amalgamation/cold vapour atomic
1157 spectrometry, Analytica Chimica Acta, 170, 337-340, 1985.

1158 Durnford, D., Dastoor, A., Figueras-Nieto, D., and Ryjkov, A.: Long range transport of
1159 mercury to the Arctic and across Canada, Atmospheric Chemistry and Physics, 10, 6063-
1160 6086, 2010.

1161 Durnford, D., Dastoor, A., Ryzhkov, A., Poissant, L., Pilote, M., and Figueras-Nieto, D.: How
1162 relevant is the deposition of mercury onto snowpacks? – Part 2: A modeling study, Atmos.
1163 Chem. Phys., 12, 9251-9274, 10.5194/acp-12-9251-2012, 2012.

1164 Ebinghaus, R., Kock, H. H., Temme, C., Einax, J. W., Löwe, A. G., Richter, A., Burrows, J.
1165 P., and Schroeder, W. H.: Antarctic springtime depletion of atmospheric mercury,
1166 Environmental Science and Technology, 36, 1238-1244, 2002.

1167 Eisele, F., Davis, D. D., Helmig, D., Oltmans, S. J., Neff, W., Huey, G., Tanner, D., Chen, G.,
1168 Crawford, J. H., Arimoto, R., Buhr, M., Mauldin, L., Hutterli, M., Dibb, J., Blake, D., Brooks,
1169 S. B., Johnson, B., Roberts, J. M., Wang, Y., Tan, D., and Flocke, F.: Antarctic tropospheric
1170 chemistry (ANTCI) 2003 overview, Atmospheric Environment, 2008, 2749-2761, 2008.

1171 Emmons, L. K., Walters, S., Hess, P. G., Lamarque, J. F., Pfister, G. G., Fillmore, D.,
1172 Granier, C., Guenther, A., Kinnison, D., Laepple, T., Orlando, J., Tie, X., Tyndall, G.,
1173 Wiedinmyer, C., Baughcum, S. L., and Kloster, S.: Description and evaluation of the Model
1174 for Ozone and Related chemical Tracers, version 4 (MOZART-4), Geosci. Model Dev., 3, 43-
1175 67, 10.5194/gmd-3-43-2010, 2010.

1176 Ferrari, C. P., Gauchard, P.-A., Aspmo, K., Dommergue, A., Magand, O., Bahlmann, E.,
1177 Nagorski, S., Temme, C., Ebinghaus, R., Steffen, A., Banic, C., Berg, T., Planchon, F.,
1178 Barbante, C., Cescon, P., and Boutron, C. F.: Snow-to-air exchanges of mercury in an arctic
1179 seasonal snowpack in Ny-Alesund, Svalbard, Atmospheric Environment, 39, 7633-7645,
1180 2005.

1181 Fisher, J. A., Jacob, D. J., Soerensen, A. L., Amos, H. M., Steffen, A., and Sunderland, E. M.:
1182 Riverine source of Arctic Ocean mercury inferred from atmospheric observations, Nature
1183 Geosci, 5, 499-504,
1184 http://www.nature.com/ngeo/journal/v5/n7/abs/ngeo1478.html#supplementary-information,
1185 2012.

1186 Fisher, J. A., Jacob, D. J., Soerensen, A. L., Amos, H. M., Corbitt, E. S., Streets, D. G., Wang,
1187 Q., Yantosca, R. M., and Sunderland, E. M.: Factors driving mercury variability in the Arctic
1188 atmosphere and ocean over the past 30 years, Global biogeochemical cycles, 27, 1226-1235,
1189 2013.

1190 Fitzgerald, W. F., and Gill, G. A.: Subnanogram determination of mercury by two-stage gold
1191 amalgamation and gas detection applied to atmospheric analysis, Analytical chemistry, 51,
1192 1714-1720, 1979.

1193 Frey, M. M., Brough, N., France, J. L., Anderson, P. S., Traulle, O., King, M. D., Jones, A.
1194 E., Wolff, E. W., and Savarino, J.: The diurnal variability of atmospheric nitrogen oxides (NO
1195 and NO2) above the Antarctic Plateau driven by atmospheric stability and snow emissions,
1196 Atmospheric Chemistry and Physics, 13, 3045-3062, 2013.

1197 Frey, M. M., Roscoe, H. K., Kukui, A., Savarino, J., France, J. L., King, M. D., Legrand, M.,
1198 and Preunkert, S.: Atmospheric nitrogen oxides (NO and NO_2) at Dome C, East Antarctica,
1199 during the OPALE campaign, Atmospheric Chemistry and Physics, 15, 7859-7875, 2015.

1200 Fujita, K., and Abe, O.: Stable isotopes in daily precipitation at Dome Fuji, East Antarctica,
1201 Geophysical research letters, 33, http://dx.doi.org/10.1029/2006GL026936, 2006.

1202 Gallée, H., and Gorodetskaya, I. V.: Validation of a limited area model over Dome C,
1203 Antarctic Plateau, during winter, Climate Dynamics, 34, 61-72, 2010.

1204 Gallée, H., Preunkert, S., Argentini, S., Frey, M. M., Genthon, C., Jourdain, B., Pietroni, I.,
1205 Casasanta, G., Barral, H., Vignon, E., Amory, C., and Legrand, M.: Characterization of the

boundary layer at Dome C (East Antarctica) during the OPALE summer campaign, Atmospheric Chemistry and Physics, 15, 6225-6236, 2015.

Gårdfeldt, K., Sommar, J., Strömberg, D., and Feng, X.: Oxidation of atomic mercury by hydroxyl radicals and photoinduced decomposition of methylmercury in the aqueous phase, Atmospheric Environment, 35, 3039-3047, 2001.

Gauchard, P.-A., Aspmo, K., Temme, C., Steffen, A., Ferrari, C., Berg, T., Ström, J., Kaleschke, L., Dommergue, A., Bahlmann, E., Magand, O., Planchon, F., Ebinghaus, R., Banic, C., Nagorski, S., Baussand, P., and Boutron, C.: Study of the origin of atmospheric mercury depletion events recorded in Ny-Ålesund, Svalbard, spring 2003, Atmospheric Environment, 39, 7620-7632, http://dx.doi.org/10.1016/j.atmosenv.2005.08.010, 2005.

Goodsite, M., Plane, J. M. C., and Skov, H.: Correction to a theoretical study of the oxidation of Hg0 to HgBr2 in the troposphere, Environmental Science & Technology, 46, 5262–5262, 2012.

Goodsite, M. E., Plane, J. M. C., and Skov, H.: A theoretical study of the oxidation of Hg^0 to $HgBr_2$ in the troposphere, Environmental Science and Technology, 38, 1772-1776, 2004.

Grannas, A. M., Jones, A. E., Dibb, J., Ammann, M., Anastasio, C., Beine, H. J., Bergin, M., Bottenheim, J., Boxe, C. S., Carver, G., Chen, G., Crawford, J. H., Domine, F., Frey, M. M., Guzman, M. I., Heard, D. E., Helmig, D., Hoffmann, M. R., Honrath, R. E., Huey, L. G., Hutterli, M., Jacobi, H.-W., Klan, P., Lefer, B., McConnell, J. R., Plane, J. M. C., Sander, R., Savarino, J., Shepson, P. B., Simpson, W. R., Sodeau, J., Von Glasow, R., Weller, R., Wolff, E. W., and Zhu, T.: An overview of snow photochemistry: evidence, mechanisms and impacts, Atmospheric Chemistry and Physics, 7, 4329-4373, 2007.

Grilli, R., Legrand, M., Kukui, A., Méjean, G., Preunkert, S., and Romanini, D.: First investigations of IO, BrO, and NO2 summer atmospheric levels at a coastal East Antarctic site using mode-locked cavity enhanced absorption spectroscopy, Geophysical research letters, 40, 791-796, 2013.

Gustin, M. S., Huang, J., Miller, M. B., Peterson, C., Jaffe, D. A., Ambrose, J., Finley, B. D., Lyman, S. N., Call, K., Talbot, R., Feddersen, D., Mao, H., and Lindberg, S. E.: Do we understand what the mercury speciation instruments are actually measuring? Results of RAMIX, Environmental Science and Technology, 47, 7295-7306, 2013.

Gustin, M. S., Amos, H. M., Huang, J., Miller, M. B., and Heidecorn, K.: Measuring and modeling mercury in the atmosphere: a critical review, Atmospheric Chemistry and Physics, 15, 5697-5713, 2015.

Gustin, M. S., Evers, D. C., Bank, M. S., Hammerschmidt, C. R., Pierce, A., Basu, N., Blum, J., Bustamante, P., Chen, C., Driscoll, C. T., Horvat, M., Jaffe, D., Pacyna, J., Pirrone, N., and Selin, N.: Importance of Integration and Implementation of Emerging and Future Mercury Research into the Minamata Convention, Environmental Science & Technology, 50, 2767-2770, 10.1021/acs.est.6b00573, 2016.

Hall, B.: The gas phase oxidation of elemental mercury by ozone, Water, Air & Soil Pollution, 80, 301-315, 1995.

Heidam, N. Z., Wåhlin, P., and Christensen, J. H.: Tropospheric Gases and Aerosols in Northeast Greenland, Journal of the Atmospheric Sciences, 56, 261-278, doi:10.1175/1520-0469(1999)056<0261:TGAAIN>2.0.CO;2, 1999.

Heidam, N. Z., Christensen, J., Wåhlin, P., and Skov, H.: Arctic atmospheric contaminants in NE Greenland: levels, variations, origins, transport, transformations and trends 1990–2001,

Science of The Total Environment, 331, 5-28, http://dx.doi.org/10.1016/j.scitotenv.2004.03.033, 2004.

Heintzenberg, J., Hansson, H. C., and Lannefors, H.: The chemical composition of arctic haze at Ny-Ålesund, Spitsbergen, Tellus, 33, 162-171, 10.1111/j.2153-3490.1981.tb01741.x, 1981.

Helmig, D., Oltmans, S. J., Carlson, D., Lamarque, J.-F., Jones, A., Labuschagne, C., Anlauf, K., and Hayden, K.: A review of surface ozone in the polar regions, Atmospheric Environment, 41, 5138-5161, 2007.

Hirdman, D., Aspmo, K., Burkhart, J. F., Eckhardt, S., Sodemann, H., and Stohl, A.: Transport of mercury in the Arctic atmosphere: Evidence for a spring-time net sink and summer-time source, Geophysical research letters, 36, doi:10.1029/2009GL038345, 2009.

Holmes, C. D., Jacob, D. J., Corbitt, E. S., Mao, J., Yang, X., Talbot, R., and Slemr, F.: Global atmospheric model for mercury including oxidation by bromine atoms, Atmospheric Chemistry and Physics, 10, 12037-12057, 2010.

Huang, J., Miller, M. B., Weiss-Penzias, P., and Gustin, M. S.: Comparison of gaseous oxidized mercury measured by KCl-coated denuders, and nylon and cation exchange membranes, Environmental Science and Technology, 47, 7307-7316, 2013.

Huang, J., Lyman, S. N., Hartman, J. S., and Gustin, M. S.: A review of passive sampling systems for ambient air mercury measurements, Environmental Science: Processes & Impacts, 16, 374-392, 10.1039/C3EM00501A, 2014.

Jaffe, D. A., Lyman, S., Amos, H. M., Gustin, M. S., Huang, J., Selin, N. E., Levin, L., Schure, A., Mason, R. P., Talbot, R., Rutter, A. P., Finley, B., Jaeglé, L., Shah, V., McClure, C., Ambrose, J., Gratz, L., Lindberg, S. E., Weiss-Penzias, P., Sheu, G.-R., Feddersen, D., Horvat, M., Dastoor, A., Hynes, A. J., Mao, H., Sonke, J. E., Slemr, F., Fisher, J. A., Ebinghaus, R., Zhang, B., and Edwards, D. P.: Progress on understanding atmospheric mercury hampered by uncertain measurements, Environmental Science and Technology, 48, 7204-7206, doi: 10.1021/es5026432, 2014.

Jin, M., Deal, C., Lee, S. H., Elliott, S., Hunke, E., Maltrud, M., and Jeffery, N.: Investigation of Arctic sea ice and ocean primary production for the period 1992–2007 using a 3-D global ice–ocean ecosystem model, Deep Sea Research Part II: Topical Studies in Oceanography, 81–84, 28-35, http://dx.doi.org/10.1016/j.dsr2.2011.06.003, 2012.

Jones, C. P., Lyman, S. N., Jaffe, D. A., Allen, T., and O'Neil, T. L.: Detection and quantification of gas-phase oxidized mercury compounds by GC/MS, Atmos. Meas. Tech., 9, 2195-2205, 10.5194/amt-9-2195-2016, 2016.

Jung, G., Hedgecock, I. M., and Pirrone, N.: ECHMERIT V1.0 – a new global fully coupled mercury-chemistry and transport model, Geosci. Model Dev., 2, 175-195, 10.5194/gmd-2-175-2009, 2009.

Kirk, J. L., St. Louis, V. L., and Sharp, M. J.: Rapid Reduction and Reemission of Mercury Deposited into Snowpacks during Atmospheric Mercury Depletion Events at Churchill, Manitoba, Canada, Environmental Science & Technology, 40, 7590-7596, doi: 10.1021/es061299+, 2006.

Koop, T., Kapilashrami, A., Molina, L. T., and Molina, M. J.: Phase transitions of sea-salt/water mixtures at low temperatures: implications for ozone chemistry in the polar marine boundary layer, Journal of geophysical research, 105, 26393–26402 10.1029/2000JD900413, 2000.

Kos, G., Ryzhkov, A., Dastoor, A., Narayan, J., Steffen, A., Ariya, P. A., and Zhang, L.: Evaluation of discrepancy between measured and modelled oxidized mercury species, Atmospheric Chemistry and Physics, 13, 4839-4863, 2013.

Kukui, A., Legrand, M., Ancellet, G., Gros, V., Bekki, S., Sarda-Estève, R., Loisil, R., and Preunkert, S.: Measurements of OH and RO2 radicals at the coastal Antarctic site of Dumont d'Urville (East Antarctica) in summer 2010-2011, Journal of geophysical research, 117, doi:10.1029/2012JD017614, 2012.

Kukui, A., Legrand, M., Preunkert, S., Frey, M. M., Loisil, R., Gil Roca, J., Jourdain, B., King, M. D., France, J. L., and Ancellet, G.: Measurements of OH and RO_2 radicals at Dome C, East Antarctica, Atmospheric Chemistry and Physics, 14, 12373-12392, 2014.

Kwon, S. Y., and Selin, N. E.: Uncertainties in Atmospheric Mercury Modeling for Policy Evaluation, Current Pollution Reports, 1-12, 10.1007/s40726-016-0030-8, 2016.

Lamborg, C. H., Hammerschmidt, C. R., Bowman, K. L., Swarr, G. J., Munson, K. M., Ohnemus, D. C., Lam, P. J., Heimbürger, L.-E., Rikjenberg, M. J. A., and Saito, M. A.: A global ocean inventory of anthropogenic mercury based on water column measurements, Nature, 512, doi:10.1038/nature13563, 2014.

Larose, C., Dommergue, A., De Angelis, M., Cossa, D., Averty, B., Marusczak, N., Soumis, N., Schneider, D., and Ferrari, C.: Springtime changes in snow chemistry lead to new insights into mercury methylation in the Arctic, Geochimica et Cosmochimica Acta, 74, 6263-6275, 2010.

Legrand, M., Preunkert, S., Jourdain, B., Gallée, H., Goutail, F., Weller, R., and Savarino, J.: Year-round record of surface ozone at coastal (Dumont d'Urville) and inland (Concordia) sites in east antarctica, Journal of geophysical research, 114, doi:10.1029/2008JD011667, 2009.

Legrand, M., Yang, X., Preunkert, S., and Theys, N.: Year-round records of sea salt, gaseous, and particulate inorganic bromine in the atmospheric boundary layer at coastal (Dumont d'Urville) and central (Concordia) East Antarctic sites, Journal of geophysical research: atmospheres, 121, DOI: 10.1002/2015JD024066, 2016a.

Legrand, M. P., S., Savarino, J., Frey, M. M., Kukui, A., Helmig, D., Jourdain, B., Jones, A., Weller, R., Brough, N., and Gallée, H.: Inter-annual variability of surface ozone at coastal (Dumont d'Urville, 2004-2014) and inland (Concordia, 2007-2014) sites in East Antarctica, Atmospheric Chemistry and Physics Discussions, doi:10.5194/acp-2016-95, in review, 2016b.

Lin, C.-J., and Pehkonen, S. O.: The chemistry of atmospheric mercury: a review, Atmospheric Environment, 33, 2067-2079, 1999.

Lin, J.-T., and McElroy, M. B.: Impacts of boundary layer mixing on pollutant vertical profiles in the lower troposphere: Implications to satellite remote sensing, Atmospheric Environment, 44, 1726-1739, http://dx.doi.org/10.1016/j.atmosenv.2010.02.009, 2010.

Lindberg, S. E., and Stratton, W. J.: Atmospheric mercury speciation: concentrations and behavior of reactive gaseous mercury in ambient air, Environmental Science and Technology, 32, 49-57, 1998.

Lindberg, S. E., Brooks, S., Lin, C.-J., Scott, K., Meyers, T., Chambers, L., Landis, M., and Stevens, R.: Formation of Reactive Gaseous Mercury in the Arctic: Evidence of Oxidation of Hg° to Gas-Phase Hg-II Compounds after Arctic Sunrise, Water, Air and Soil Pollution: Focus, 1, 295-302, doi: 10.1023/a:1013171509022, 2001.

Lindberg, S. E., Brooks, S., Lin, C.-J., Scott, K. J., Landis, M. S., Stevens, R. K., Goodsite, M. E., and Richter, A.: Dynamic oxidation of gaseous mercury in the arctic troposphere at polar sunrise, Environmental Science and Technology, 36, 1245-1256, 2002.

Lindqvist, O., and Rodhe, H.: Atmospheric mercury - a review, Tellus, 37B, 136-159, 1985.

Liu, G.: Deriving snow cloud characteristics from CloudSat observations, Journal of geophysical research, 113, http://dx.doi.org/10.1029/2007JD009766, 2008.

Lu, J. Y., Schroeder, W. H., Barrie, L. A., Steffen, A., Welch, H. E., Martin, K., Lockhart, L., Hunt, R. V., Boila, G., and Richter, A.: Magnification of atmospheric mercury deposition to polar regions in springtime: the link to tropospheric ozone depletion chemistry, Geophysical research letters, 28, 3219-3222, 2001.

Lyman, S. N., Jaffe, D. A., and Gustin, M. S.: Release of mercury halides from KCl denuders in the presence of ozone, Atmospheric Chemistry and Physics, 10, 8197-8204, 2010.

Lynch, J. A., Horner, K. S., and Grimm, J. W.: Atmospheric deposition: spatial and temporal variations in Pennsylvania 2002, Penn State Institutes of the Environment, The Pennsylvania State University, University Park, PA, 231, 2003.

Maturilli, M., Herber, A., and König-Langlo, G.: Climatology and time series of surface meteorology in Ny-Alesund, Svalbard, Earth System Science Data, 5, 155-163, 10.5194/essd-5-155-2013, 2013.

Moore, C. W., Obrist, D., Steffen, A., Staebler, R. M., Douglas, T. A., Richter, A., and Nghiem, S. V.: Convective forcing of mercury and ozone in the Arctic boundary layer induced by leads in sea ice, Nature, 506, 81-84, 10.1038/nature12924, 2014.

Munthe, J.: The aqueous oxidation of elemental mercury by ozone, Atmospheric Environment, 26, 1461-1468, 1992.

Nash, J. E., and Sutcliffe, J. V.: River flow forecasting through conceptual models part I — A discussion of principles, Journal of Hydrology, 10, 282-290, http://dx.doi.org/10.1016/0022-1694(70)90255-6, 1970.

Neff, W., Helmig, D., Grachev, A. A., and Davis, D.: A study of boundary layer behavior associated with high NO concentrations at the South Pole using a minisodar, tethered balloon, and sonic anemometer, Atmospheric Environment, 42, 2762-2779, 2008.

Nerentorp Mastromonaco, M., Gårdfeldt, K., Jourdain, B., Abrahamsson, K., Granfors, A., Ahnoff, M., Dommergue, A., Méjean, G., and Jacobi, H.-W.: Antarctic winter mercury and ozone depletion events over sea ice, Atmospheric Environment, 129, 125-132, 2016.

Neuman, J. A., Nowak, J. B., Huey, L. G., Burkholder, J. B., Dibb, J. E., Holloway, J. S., Liao, J., Peischl, J., Roberts, J. M., Ryerson, T. B., Scheuer, E., Stark, H., Stickel, R. E., Tanner, D. J., and Weinheimer, A.: Bromine measurements in ozone depleted air over the Arctic Ocean, Atmos. Chem. Phys., 10, 6503-6514, 10.5194/acp-10-6503-2010, 2010.

Nguyen, Q. T., Skov, H., Sørensen, L. L., Jensen, B. J., Grube, A. G., Massling, A., Glasius, M., and Nøjgaard, J. K.: Source apportionment of particles at Station Nord, North East Greenland during 2008–2010 using COPREM and PMF analysis, Atmos. Chem. Phys., 13, 35-49, 10.5194/acp-13-35-2013, 2013.

O'Driscoll, N. J., Siciliano, S. D., Lean, D. R. S., and Amyot, M.: Gross photoreduction kinetics of mercury in temperate freshwater lakes and rivers: application to a general model of DGM dynamics, Environmental Science and Technology, 40, 837-843, 2006.

Palerme, C., Kay, J. E., Genthon, C., L'Ecuyer, T., Wood, N. B., and Claud, C.: How much snow falls on the Antarctic ice sheet?, The Cryosphere, 8, 1577-1587, 10.5194/tc-8-1577-2014, 2014.

Parish, T. R., and Bromwich, D. H.: The surface windfield over the Antarctic ice sheets, Nature, 328, 51-54, 1987.

Parish, T. R., and Bromwich, D. H.: Reexamination of the near-surface airflow over the Antarctic continent and implications on atmospheric circulations at high southern latitudes, Monthly Weather Review, 135, 1961-1973, 2007.

Parrella, J. P., Jacob, D. J., Liang, Q., Zhang, Y., Mickley, L. J., Miller, B., Evans, M. J., Yang, X., Pyle, J. A., Theys, N., and Van Roozendael, M.: Tropospheric bromine chemistry: implications for present and pre-industrial ozone and mercury, Atmospheric Chemistry and Physics, 12, 6723-6740, 2012.

Petersen, G., Munthe, J., Pleijel, K., Bloxam, R., and Kumar, A. V.: A comprehensive Eulerian modeling framework for airborne mercury species: Development and testing of the Tropospheric Chemistry module (TCM), Atmospheric Environment, 32, 829-843, http://dx.doi.org/10.1016/S1352-2310(97)00049-6, 1998.

Pfaffhuber, K. A., Berg, T., Hirdman, D., and Stohl, A.: Atmospheric mercury observations from Antarctica: seasonal variation and source and sink region calculations, Atmospheric Chemistry and Physics, 12, 3241-3251, 2012.

Pietroni, I., Argentini, S., Petenko, I., and Sozzi, R.: Measurements and parametrizations of the atmospheric boundary-layer height at Dome C, Antarctica, Boundary-Layer Meteorology, 143, 189-206, 2012.

Platt, U., and Janssen, C.: Observation and role of the free radicals NO_3, ClO, BrO and IO in the troposphere, Faraday Discuss., 100, 175-198, 1995.

Poissant, L., and Pilote, M.: Time series analysis of atmospheric mercury in Kuujjuarapik/Whapmagoostui (Québec), J. Phys. IV France, 107, 1079-1082, 2003.

Poulain, A. J., Lalonde, J. D., Amyot, M., Shead, J. A., Raofie, F., and Ariya, P. A.: Redox transformations of mercury in an Arctic snowpack at springtime, Atmospheric Environment, 38, 6763-6774, 2004.

Prestbo, E. M., and Gay, D. A.: Wet deposition of mercury in the U.S. and Canada, 1996–2005: Results and analysis of the NADP mercury deposition network (MDN), Atmospheric Environment, 43, 4223-4233, http://dx.doi.org/10.1016/j.atmosenv.2009.05.028, 2009.

Saiz-Lopez, A., Mahajan, A. S., Salmon, R. A., Bauguitte, S. J.-B., Jones, A. E., Roscoe, H. K., and Plane, J. M. C.: Boundary layer halogens in coastal antarctica, Science, 317, 348-351, 2007.

Sander, R., Burrows, J., and Kaleschke, L.: Carbonate precipitation in brine – a potential trigger for tropospheric ozone depletion events, Atmos. Chem. Phys., 6, 4653-4658, 10.5194/acp-6-4653-2006, 2006.

Savarino, J., Kaiser, J., Morin, S., Sigman, D. M., and Thiemens, M. H.: Nitrogen and oxygen isotopic constraints on the origin of atmospheric nitrate in coastal Antarctica, Atmospheric Chemistry and Physics, 7, 1925-1945, 2007.

Schroeder, W. H., Anlauf, K. G., Barrie, L. A., Lu, J. Y., Steffen, A., Schneeberger, D. R., and Berg, T.: Arctic spingtime depletion of mercury, Nature, 394, 331-332, 1998.

Selin, N. E., Jacob, D. J., Yantosca, R. M., Strode, S., Jaeglé, L., and Sunderland, E. M.: Global 3-D land-ocean-atmosphere model for mercury: present-day versus preindustrial cycles and anthropogenic enrichment factors for deposition, Global biogeochemical cycles, 22, doi:10.1029/2007GB003040, 2008.

Selin, N. E.: Global biogeochemical cycling of mercury: a review, Annual Review of Environment and Resources, 34, 43-63, 2009.

Shaw, G. E.: Evidence for a central Eurasian source area of Arctic haze in Alaska, Nature, 299, 815-818, 10.1038/299815a0, 1982.

Skamarock, W. C., Klemp, J. B., Dudhia, J., Gill, D. O., Barker, D. M., Wang, W., and Powers, J. G.: A description of the advanced research WRF version 2. NCAR/TN-468+STR. NCAR Technical Note. Boulder, CO, USA, 2007.

Skov, H., Christensen, J. H., Goodsite, M. E., Heidam, N. Z., Jensen, B., Wåhlin, P., and Geernaert, G.: Fate of Elemental Mercury in the Arctic during Atmospheric Mercury Depletion Episodes and the Load of Atmospheric Mercury to the Arctic, Environmental Science & Technology, 38, 2373-2382, 10.1021/es030080h, 2004.

Slemr, F., Angot, H., Dommergue, A., Magand, O., Barret, M., Weigelt, A., Ebinghaus, R., Brunke, E.-G., Pfaffhuber, K. A., Edwards, G., Howard, D., Powell, J., Keywood, M., and Wang, F.: Comparison of mercury concentrations measured at several sites in the Southern Hemisphere, Atmospheric Chemistry and Physics, 15, 3125-3133, 2015.

Soerensen, A. L., Sunderland, E. M., Holmes, C. D., Jacob, D. J., Yantosca, R. M., Skov, H., Christensen, J. H., Strode, S. A., and Mason, R. P.: An improved global model for air-sea exchange of mercury: high concentrations over the north atlantic, Environmental Science and Technology, 44, 8574-8580, 2010.

Soerensen, A. L., Jacob, D. J., Schartup, A. T., Fisher, J. A., Lehnherr, I., St. Louis, V. L., Heimbürger, L.-E., Sonke, J. E., Krabbenhoft, D. P., and Sunderland, E. M.: A mass budget for mercury and methylmercury in the Arctic Ocean, Global biogeochemical cycles, 30, 10.1002/2015GB005280, 2016.

Sommar, J., Gårdfeldt, K., Strömberg, D., and Feng, X.: A kinetic study of the gas-phase reactions between the hydroxyl radical and atomic mercury, Atmospheric Environment, 35, 3049-3054, 2001.

Sommar, J., Wängberg, I., Berg, T., Gårdfeldt, K., Munthe, J., Richter, A., Urba, A., Wittrock, F., and Schroeder, W. H.: Circumpolar transport and air-surface exchange of atmospheric mercury at Ny-Alesund (79°N), Svalbard, spring 2002, Atmos. Chem. Phys., 7, 151-166, 10.5194/acp-7-151-2007, 2007.

Sommar, J., Andersson, M. E., and Jacobi, H. W.: Circumpolar measurements of speciated mercury, ozone and carbon monoxide in the boundary layer of the Arctic Ocean, Atmos. Chem. Phys., 10, 5031-5045, 10.5194/acp-10-5031-2010, 2010.

Song, S., Selin, N. E., Soerensen, A. L., Angot, H., Artz, R., Brooks, S., Brunke, E.-G., Conley, G., Dommergue, A., Ebinghaus, R., Holsen, T. M., Jaffe, D. A., Kang, D., Kelley, P., Luke, W. T., Magand, O., Marumoto, K., Pfaffhuber, K. A., Ren, X., Sheu, G.-R., Slemr, F., Warneke, T., Weigelt, A., Weiss-Penzias, P., Wip, D. C., and Zhang, Q.: Top-down constraints on atmospheric mercury emissions and implications for global biogeochemical cycling, Atmospheric Chemistry and Physics, 15, 7103-7125, 2015.

1467 Spreen, G., Kaleschke, L., and Heygster, G.: Sea ice remote sensing using AMSR-E 89 GHz
1468 channels, Journal of geophysical research, 113, http://dx.doi.org/10.1029/2005JC003384,
1469 2008.

1470 Sprovieri, F., Pirrone, N., Hedgecock, I. M., Landis, M. S., and Stevens, R. K.: Intensive
1471 atmospheric mercury measurements at Terra Nova Bay in antarctica during November and
1472 December 2000, Journal of geophysical research, 107, 4722, 2002.

1473 Sprovieri, F., Pirrone, N., Landis, M. S., and Stevens, R. K.: Oxidation of Gaseous Elemental
1474 Mercury to Gaseous Divalent Mercury during 2003 Polar Sunrise at Ny-Alesund,
1475 Environmental Science & Technology, 39, 9156-9165, 10.1021/es050965o, 2005a.

1476 Sprovieri, F., Pirrone, N., Landis, M. S., and Stevens, R. K.: Atmospheric mercury behavior at
1477 different altitudes at Ny Alesund during Spring 2003, Atmospheric Environment, 39, 7646-
1478 7656, http://dx.doi.org/10.1016/j.atmosenv.2005.08.001, 2005b.

1479 Sprovieri, F., Pirrone, N., Ebinghaus, R., Kock, H. H., and Dommergue, A.: A review of
1480 worldwide atmospheric mercury measurements, Atmospheric Chemistry and Physics, 10,
1481 8245-8265, 2010.

1482 Sprovieri, F., Pirrone, N., Bencardino, M., D'Amore, F., Cinnirella, S., Esposito, G., Landis,
1483 M., Ebinghaus, R., Weigelt, A., Brunke, E.-G., Martin, L., Munthe, J., Wängberg, I., Artaxo,
1484 P., Morais, F., Cairns, W., Barbante, C., Diéguez, M., Garcia, P. E., Dommergue, A., Angot,
1485 H., Magand, O., Skov, H., Horvat, M., Kotnik, J., Read, K. A., Neves, M., Gawlik, B. M.,
1486 Sena, F., Mashyanov, N., Wip, D. C., Feng, S. X., Hui, Z., Ramachandran, R., Cossa, D.,
1487 Knoery, J., and Marusczak, N.: Atmospheric mercury concentrations observed at ground-
1488 based monitoring sites globally distributed in the framework of the GMOS network, this
1489 issue-a.

1490 Sprovieri, F., Pirrone, N., Bencardino, M., D'Amore, F., Wangberg, I., Munthe, J., Ebinghaus,
1491 R., Weigelt, A., Brunke, E.-G., Martin, A. P., Dommergue, A., Angot, H., Magand, O.,
1492 Barbante, C., Cairns, W., Gawlik, B. M., Sena, F., Vardè, M., Horvat, M., Kotnik, J.,
1493 Dieguez, M., Feng, S. X., Hui, Z., and Mashyanov, N.: Five-year records of total mercury
1494 deposition fluxes at GMOS sites in the Northern and Southern Hemispheres, this issue-b.

1495 Steen, A. O., Berg, T., Dastoor, A. P., Durnford, D. A., Hole, L. R., and Pfaffhuber, K. A.:
1496 Dynamic exchange of gaseous elemental mercury during polar night and day, Atmospheric
1497 Environment, 43, 5604-5610, http://dx.doi.org/10.1016/j.atmosenv.2009.07.069, 2009.

1498 Steen, A. O., Berg, T., Dastoor, A. P., Durnford, D. A., Engelsen, O., Hole, L. R., and
1499 Pfaffhuber, K. A.: Natural and anthropogenic atmospheric mercury in the European Arctic: a
1500 fractionation study, Atmos. Chem. Phys., 11, 6273-6284, 10.5194/acp-11-6273-2011, 2011.

1501 Steffen, A., Schroeder, W., Bottenheim, J., Narayan, J., and Fuentes, J. D.: Atmospheric
1502 mercury concentrations: measurements and profiles near snow and ice surfaces in the
1503 Canadian Arctic during Alert 2000, Atmospheric Environment, 36, 2653-2661, 2002.

1504 Steffen, A., Schroeder, W. H., Edwards, G., and Banic, C.: Mercury throughout polar sunrise
1505 2002, J. Phys. IV France, 107, 1267-1270, 2003.

1506 Steffen, A., Schroeder, W., Macdonald, R., Poissant, L., and Konoplev, A.: Mercury in the
1507 Arctic atmosphere: An analysis of eight years of measurements of GEM at Alert (Canada) and
1508 a comparison with observations at Amderma (Russia) and Kuujjuarapik (Canada), Science of
1509 The Total Environment, 342, 185-198, http://dx.doi.org/10.1016/j.scitotenv.2004.12.048,
1510 2005.

1511 Steffen, A., Douglas, T., Amyot, M., Ariya, P. A., Aspmo, K., Berg, T., Bottenheim, J.,
1512 Brooks, S., Cobbett, F., Dastoor, A., Dommergue, A., Ebinghaus, R., Ferrari, C., Gardfeldt,
1513 K., Goodsite, M. E., Lean, D., Poulain, A. J., Scherz, C., Skov, H., Sommar, J., and Temme,
1514 C.: A synthesis of atmospheric mercury depletion event chemistry in the atmosphere and
1515 snow, Atmospheric Chemistry and Physics, 8, 1445-1482, 2008.

1516 Steffen, A., Scherz, T., Oslon, M., Gay, D. A., and Blanchard, P.: A comparison of data
1517 quality control protocols for atmospheric mercury speciation measurements, Journal of
1518 Environmental Monitoring, 14, 752-765, doi: 10.1039/c2em10735j, 2012.

1519 Steffen, A., Bottenheim, J., Cole, A., Ebinghaus, R., Lawson, G., and Leaitch, W. R.:
1520 Atmospheric mercury speciation and mercury in snow over time at Alert, Canada,
1521 Atmospheric Chemistry and Physics, 14, 2219-2231, 2014.

1522 Steffen, A., Lehnherr, I., Cole, A., Ariya, P., Dastoor, A., Durnford, D., Kirk, J., and Pilote,
1523 M.: Atmospheric mercury in the Canadian Arctic. Part I: A review of recent field
1524 measurements, Science of The Total Environment, 509–510, 3-15,
1525 http://dx.doi.org/10.1016/j.scitotenv.2014.10.109, 2015.

1526 Stephens, G. L., Vane, D. G., Tanelli, S., Eastwood, I., Durden, S., Rokey, M., Reinke, D.,
1527 Partain, P., Mace, G. G., Austin, R., L'Ecuyer, T., Haynes, J., Lebsock, M., Suzuki, K.,
1528 Waliser, D., Wu, D., Kay, J., Gettelman, A., Wang, Z., and Marchand, R.: CloudSat mission:
1529 performance and early science after the first year of operation, Journal of geophysical
1530 research, 113, http://dx.doi.org/10.1029/2008JD009982, 2008.

1531 Subir, M., Ariya, P. A., and Dastoor, A.: A review of uncertainties in atmospheric modeling
1532 of mercury chemistry I. Uncertainties in existing kinetic parameters - fundamental limitations
1533 and the importance of heteregeneous chemistry, Atmospheric Environment, 45, 5664-5675,
1534 2011.

1535 Subir, M., Ariya, P. A., and Dastoor, A.: A review of the sources of uncertainties in
1536 atmospheric mercury modeling II. Mercury surface and heterogeneous chemistry - a missing
1537 link, Atmospheric Environment, 46, 1-10, 2012.

1538 Tarasick, D. W., and Bottenheim, J. W.: Surface ozone depletion episodes in the Arctic and
1539 Antarctic from historical ozonesonde records, Atmos. Chem. Phys., 2, 197-205, 10.5194/acp-
1540 2-197-2002, 2002.

1541 Tekran: Tekran 2537 mercury monitor detection limit. Summary of known estimates, Tekran
1542 Instruments Corp., Toronto, ON, Canada., 2011.

1543 Temme, C., Einax, J. W., Ebinghaus, R., and Schroeder, W. H.: Measurements of atmospheric
1544 mercury species at a coastal site in the antarctic and over the atlantic ocean during polar
1545 summer, Environmental Science and Technology, 37, 22-31, 2003.

1546 Theys, N., Van Roozendael, M., Hendrick, F., Yang, X., De Smedt, I., Richter, A., Begoin,
1547 M., Errera, Q., Johnston, P. V., Kreher, K., and De Mazière, M.: Global observations of
1548 tropospheric BrO columns using GOME-2 satellite data, Atmospheric Chemistry and Physics,
1549 11, 1791-1811, 2011.

1550 Tossell, J. A.: Calculation of the energetics for oxidation of gas-phase elemental Hg by Br and
1551 BrO, The Journal of physical chemistry A, 107, 7804-7808, 2003.

1552 Toyota, K., Dastoor, A., and Ryzhkov, A.: Air-snowpack exchange of bromine, ozone and
1553 mercury in the springtime Arctic simulated by the 1-D model PHANTAS - Part 2: mercury
1554 and its speciation, Atmospheric Chemistry and Physics, 14, 4135-4167, 2014.

Travnikov, O., and Ilyin, I.: The EMEP/MSC-E Mercury Modelling System, in: Mercury Fate and Transport in the Global Atmosphere: Emissions, Measurements, and Models, edited by: Pirrone, N., and Mason, R. P., Springer, 571-587, 2009.

Travnikov, O., Dastoor, A., De Simone, F., Hedgecock, I. M., Pirrone, N., Ryjkov, A., Selin, N. E., Song, S., and Yang, X.: Multi-model study of mercury dispersion in the atmosphere: Atmospheric processes and model evaluation, in preparation.

UNEP: Text of the Minamata Convention on Mercury for adoption by the Conference of Plenipotentiaries. unep.org. July 31, Available at: http://www.unep.org/hazardoussubstances/Portals/9/Mercury/Documents/dipcon/CONF_3_Minamata%20Convention%20on%20Mercury_final%2026%2008_e.pdf, last access: 27 March 2016, 2013a.

UNEP: Global Mercury Assessment 2013: Sources, Emissions, Releases and Environmental Transport. UNEP Chemicals Branch, Geneva, Switzerland, 44 pp., 2013b.

UNEP: Global mercury modelling: update of modelling results in the global mercury assessment 2013, 2015.

Wang, J., Zhang, L., and Xie, Z.: Total gaseous mercury along a transect from coastal to central Antarctic: Spatial and diurnal variations, Journal of Hazardous Materials, http://dx.doi.org/10.1016/j.jhazmat.2016.05.068, 2016.

Wang, P.: Atmospheric mercury speciation and aerosol properties at Ny-Alesund, Department of Chemistry, Norwegian University of Science and Technology, 130 pp., 2015.

Yang, X., Cox, R. A., Warwick, N. J., Pyle, J. A., Carver, G. D., O'Connor, F. M., and Savage, N. H.: Tropospheric bromine chemistry and its impacts on ozone: A model study, Journal of geophysical research, 110, 10.1029/2005JD006244, 2005.

Yu, J., Xie, Z., Kang, H., Li, Z., Sun, C., Bian, L., and Zhang, P.: High variability of atmospheric mercury in the summertime boundary layer through the central Arctic Ocean, Scientific Reports, 4, 6091, 10.1038/srep06091

http://www.nature.com/articles/srep06091#supplementary-information, 2014.

Zambrano-Bigiarini, M.: hydroGOF: Goodness-of-fit functions for comparison of simulated and observed hydrological time series. R package version 0.3-8. http://CRAN.R-project.org/package=hydroGOF, 2014.

Zatko, M., Geng, L., Alexander, B., Sofen, E., and Klein, K.: The impact of snow nitrate photolysis on boundary layer chemistry and the recycling and redistribution of reactive nitrogen across Antarctica and Greenland in a global chemical transport model, Atmos. Chem. Phys., 16, 2819-2842, 10.5194/acp-16-2819-2016, 2016.

Zatko, M. C., Grenfell, T. C., Alexander, B., Doherty, S. J., Thomas, J. L., and Yang, X.: The influence of snow grain size and impurities on the vertical profiles of actinic flux and associated NOx emissions on the Antarctic and Greenland ice sheets, Atmospheric Chemistry and Physics, 13, 3547-3567, 2013.

Zhu, W., Lin, C. J., Wang, X., Sommar, J., Fu, X., and Feng, X.: Global observations and modeling of atmosphere–surface exchange of elemental mercury: a critical review, Atmos. Chem. Phys., 16, 4451-4480, 10.5194/acp-16-4451-2016, 2016.

	Code	Elevation (m a.s.l.)	Analyte	Instrumentation	Flow rate (L/min)	Resolution	Filter at the inlet	Sampling line
Arctic	ALT	195	Hg(0)	Tekran 2537A	1.0	5 min	speciation unit	heated
			Hg(p), RGM	Tekran 2537A/1130/1135	10.0	2 h		
	SND	30	Hg(0)	Tekran 2537A	1.5	5 min	sodalime	heated
	NYA	474	Hg(0)	Tekran 2537A	1.5	5 min	2 µm PTFE and sodalime	heated
	AND	10	Hg(0)	Tekran 2537A	1.5	5 min	2 µm PTFE and sodalime	heated
Antarctica	TR	1275	Hg(0)	Tekran 2537A	1.5	5 min	2 µm PTFE filter	unheated
	DC	3220	Hg(0)	Tekran 2537A	0.8	5-15 min	0.45 µm PTFE filter	unheated
	DDU	43	Hg(0)	Tekran 2537B	1.0	10-15 min	0.20 µm PTFE filter	unheated
	ANT	20	Hg(0)	Tekran 2537A	1.0	5 min	speciation unit	heated
			Hg(p), RGM	Tekran 2537A/1130/1135	10.0	2 h		
	OSO	15	Hg(0)	Tekran 2537A	1.0	5 min	0.45 µm PTFE filter	unheated

Table 1: Summary of the instrumentation used at the various Polar sites to measure atmospheric mercury species.

	Station	2011				2012				2013				2014				2015			
		n	mean	median	SD	n	mean	median	SD	n	mean	median	SD	n	mean	median	SD	n	mean	median	SD
Arctic	ALT	8040	1.39	1.35	0.45	8447	1.21	1.21	0.35	8048	1.31	1.39	0.46	8358	1.45	1.45	0.33	na	na	na	na
	SND	4712	1.26	1.34	0.32	7932	1.44	1.44	0.26	6605	1.57	1.49	0.44	4991	1.36	1.36	0.35	1059	1.11	1.11	0.32
	NYA	8173	1.51	1.59	0.31	8181	1.51	1.54	0.21	6980	1.47	1.52	0.30	6730	1.48	1.57	0.33	8342	1.49	1.49	0.21
	AND	7444	1.61	1.61	0.15	8428	1.61	1.61	0.13	7862	1.53	1.56	0.15	8146	1.50	1.51	0.16	7146	1.50	1.50	0.10
Antarctica	TR	5978	0.95	0.99	0.20	7808	0.98	0.97	0.15	8197	0.90	0.93	0.15	7421	0.95	1.00	0.21	3670	0.94	0.93	0.31
	DC	na	na	na	na	3761	0.76	0.70	0.24	2900	0.84	0.87	0.27	na	na	na	na	8383	1.06	1.12	0.41
	DDU	na	na	na	na	5949	0.91	0.92	0.20	5121	0.85	0.85	0.19	1958	0.85	0.82	0.38	3114	0.86	0.87	0.19

Table 2: Annually-based statistics (number of hourly-averaged data (n), mean, median, standard deviation (SD)) of Hg(0) concentrations (in ng m^{-3}) at ground-based Polar sites over the 2011-2015 period. Note that 2013 data at DC refer to concentrations recorded at 210 cm above the snowpack. The 2015 data coverage is May to June at SND and January to May at DDU (see Table 3). na: not available due to QA/QC invalidation, instrument failure, or because the QA/QC validation is currently in progress (2015 data).

	ALT				SND				NYA				AND				TR				DC				DDU			
	n	mean	median	SD	n	mean	median	SD	n	mean	median	SD	n	mean	median	SD	n	mean	median	SD	n	mean	median	SD	n	mean	median	SD
2011																												
Jan	736	1.44	1.44	0.06	698	1.46	1.46	0.07	739	1.49	1.58	0.26	627	1.72	1.71	0.14	671	0.85	0.86	0.25	na	na	na	na	na	na	na	na
Feb	664	1.35	1.39	0.22	631	1.40	1.40	0.08	661	1.48	1.55	0.31	446	1.72	1.73	0.14	656	0.98	1.06	0.25	na	na	na	na	na	na	na	na
Mar	740	1.33	1.35	0.33	613	1.24	1.30	0.28	548	1.43	1.59	0.38	673	1.71	1.73	0.21	735	1.06	1.05	0.11	na	na	na	na	na	na	na	na
Apr	720	0.87	0.91	0.52	621	1.05	1.13	0.36	719	1.58	1.65	0.31	631	1.59	1.59	0.16	711	1.01	1.01	0.05	na	na	na	na	na	na	na	na
May	647	1.38	1.28	0.73	622	0.91	0.91	0.44	709	1.17	1.18	0.42	494	1.42	1.41	0.13	718	0.99	0.99	0.03	na	na	na	na	na	na	na	na
Jun	690	1.87	1.85	0.31	434	1.27	1.21	0.35	716	1.46	1.58	0.28	658	1.53	1.53	0.11	614	0.98	0.99	0.04	na	na	na	na	na	na	na	na
Jul	672	1.96	1.97	0.48	na	na	na	na	647	1.77	1.73	0.27	676	1.55	1.54	0.09	733	0.98	0.98	0.05	na	na	na	na	na	na	na	na
Aug	724	1.62	1.63	0.19	na	na	na	na	663	1.66	1.68	1.15	606	1.52	1.53	0.08	169	0.92	0.92	0.04	na	na	na	na	na	na	na	na
Sep	670	1.21	1.20	0.06	458	1.30	1.30	0.04	715	1.66	1.66	0.12	444	1.58	1.59	0.09	na	na	na	na	na	na	na	na	na	na	na	na
Oct	719	1.16	1.16	0.02	107	1.23	1.23	0.03	669	1.59	1.60	0.12	728	1.62	1.64	0.10	na	na	na	na	na	na	na	na	na	na	na	na
Nov	395	1.20	1.21	0.06	na	na	na	na	681	1.32	1.34	0.30	719	1.64	1.62	0.11	254	0.59	0.71	0.34	na	na	na	na	na	na	na	na
Dec	663	1.29	1.30	0.06	528	1.52	1.53	0.05	706	1.59	1.59	0.06	742	1.71	1.71	0.06	717	0.87	0.86	0.29	na	na	na	na	na	na	na	na
2012																												
Jan	595	1.33	1.36	0.10	744	1.53	1.53	0.07	595	1.62	1.61	0.06	720	1.75	1.74	0.07	497	1.07	1.08	0.28	259	0.61	0.57	0.33	576	1.06	1.09	0.32
Feb	685	1.32	1.33	0.07	696	1.48	1.49	0.07	696	1.59	1.59	0.06	696	1.76	1.75	0.05	660	1.03	1.00	0.23	593	0.93	1.00	0.42	670	1.01	1.03	0.23
Mar	722	0.92	1.02	0.41	744	1.26	1.35	0.29	726	1.48	1.59	0.28	744	1.73	1.73	0.08	744	0.97	0.97	0.05	67	1.14	1.14	0.26	635	0.97	0.95	0.09
Apr	695	0.79	0.75	0.49	319	1.29	1.32	0.41	550	1.31	1.45	0.37	720	1.59	1.60	0.12	712	0.97	0.96	0.04	na	na	na	na	668	0.97	0.98	0.08
May	698	1.19	1.27	0.59	703	1.58	1.63	0.52	697	1.39	1.46	0.26	744	1.55	1.59	0.16	649	0.97	0.97	0.03	na	na	na	na	696	0.92	0.94	0.11
Jun	720	1.52	1.52	0.24	719	1.61	1.60	0.22	698	1.52	1.50	0.10	720	1.56	1.57	0.09	654	0.95	0.94	0.04	423	0.82	0.81	0.06	663	0.88	0.88	0.08
Jul	728	1.50	1.44	0.33	744	1.61	1.59	0.22	734	1.68	1.68	0.17	412	1.61	1.61	0.07	487	0.87	0.87	0.06	624	0.70	0.70	0.05	101	0.79	0.79	0.07
Aug	744	1.27	1.26	0.09	593	1.54	1.53	0.12	678	1.70	1.69	0.09	744	1.52	1.52	0.06	670	1.01	1.02	0.07	682	0.66	0.67	0.05	107	0.63	0.62	0.05
Sep	657	1.16	1.16	0.06	631	1.43	1.42	0.07	713	1.58	1.56	0.10	720	1.46	1.45	0.07	612	1.08	1.08	0.08	682	0.72	0.66	0.14	131	0.99	1.00	0.09
Oct	742	1.16	1.16	0.04	601	1.28	1.27	0.06	664	1.38	1.39	0.05	744	1.56	1.56	0.10	744	1.02	1.01	0.12	431	0.79	0.81	0.20	719	0.82	0.84	0.14
Nov	718	1.16	1.17	0.06	694	1.31	1.28	0.09	700	1.40	1.41	0.08	720	1.57	1.57	0.07	699	0.94	0.94	0.15	na	na	na	na	428	0.76	0.74	0.24
Dec	743	1.16	1.18	0.05	744	1.29	1.27	0.11	730	1.45	1.47	0.15	744	1.70	1.67	0.09	680	0.90	0.88	0.22	na	na	na	na	555	0.82	0.8	0.21
2013																												
Jan	468	1.25	1.27	0.12	729	1.5	1.51	0.13	483	1.52	1.54	0.13	717	1.66	1.66	0.05	711	0.97	0.96	0.24	762	0.69	0.64	0.30	644	0.88	0.84	0.37
Feb	671	1.23	1.27	0.14	378	1.46	1.45	0.06	596	1.65	1.67	0.10	671	1.68	1.67	0.06	665	0.93	0.97	0.21	585	0.68	0.59	0.41	450	0.81	0.81	0.23
Mar	664	1.14	1.28	0.40	na	na	na	na	671	1.39	1.45	0.30	725	1.57	1.59	0.07	727	0.98	1.00	0.08	487	1.16	1.15	0.19	215	0.81	0.77	0.15
Apr	707	0.65	0.60	0.49	582	1.43	1.38	0.63	689	1.22	1.40	0.51	680	1.46	1.49	0.20	704	0.98	0.97	0.05	271	1.16	1.14	0.16	635	0.96	0.95	0.04
May	739	0.91	0.87	0.67	744	1.39	1.23	0.75	744	1.40	1.48	0.33	732	1.41	1.40	0.10	688	0.94	0.94	0.03	464	1.01	0.99	0.10	725	0.88	0.88	0.04
Jun	696	1.43	1.53	0.59	719	1.89	1.96	0.50	686	1.45	1.63	0.42	713	1.41	1.43	0.13	718	0.95	0.95	0.02	297	0.93	0.93	0.05	661	0.83	0.83	0.05
Jul	742	1.82	1.80	0.23	709	1.97	1.95	0.28	206	1.52	1.50	0.13	717	1.43	1.45	0.12	713	0.96	0.96	0.03	554	0.89	0.89	0.05	639	0.80	0.81	0.09
Aug	720	1.71	1.67	0.15	538	1.84	1.76	0.23	716	1.63	1.60	0.12	622	1.42	1.43	0.11	679	0.90	0.91	0.05	591	0.75	0.75	0.08	655	0.73	0.73	0.10
Sep	720	1.43	1.41	0.04	412	1.47	1.49	0.13	690	1.51	1.51	0.07	266	1.50	1.49	0.08	670	0.87	0.87	0.06	616	0.85	0.85	0.08	82	0.68	0.68	0.06
Oct	744	1.36	1.36	0.04	502	1.41	1.40	0.05	687	1.48	1.48	0.06	739	1.56	1.56	0.05	710	0.79	0.76	0.12	245	0.75	0.79	0.17	na	na	na	na
Nov	605	1.36	1.36	0.02	597	1.40	1.39	0.07	298	1.40	1.41	0.07	545	1.60	1.61	0.05	606	0.76	0.76	0.18	431	0.66	0.60	0.33	na	na	na	na
Dec	646	1.32	1.33	0.07	694	1.36	1.36	0.09	514	1.52	1.44	0.31	735	1.69	1.69	0.05	606	0.78	0.76	0.20	213	0.84	0.85	0.24	415	0.98	0.97	0.25
2014																												
Jan	743	1.47	1.47	0.07	719	1.41	1.37	0.16	701	1.44	1.60	0.36	688	1.69	1.68	0.04	427	0.70	0.62	0.31	na	na	na	na	585	0.91	0.92	0.33
Feb	671	1.48	1.52	0.16	672	1.42	1.46	0.23	584	1.69	1.67	0.10	656	1.66	1.66	0.06	414	0.89	0.90	0.17	na	na	na	na	26	0.42	0.41	0.13
Mar	744	1.49	1.59	0.31	694	1.34	1.34	0.33	703	1.55	1.64	0.24	718	1.62	1.61	0.07	708	1.09	1.09	0.16	na	na	na	na	na	na	na	na
Apr	675	1.42	1.45	0.60	718	1.21	1.21	0.47	688	1.31	1.49	0.49	677	1.52	1.52	0.11	681	1.06	1.07	0.04	na	na	na	na	50	0.97	0.98	0.04
May	702	1.21	1.29	0.50	722	1.56	1.60	0.50	709	1.13	1.33	0.54	534	1.27	1.28	0.26	542	1.07	1.08	0.05	na	na	na	na	84	0.68	0.63	0.10
Jun	712	1.43	1.58	0.39	718	1.46	1.45	0.25	689	1.49	1.56	0.25	664	1.41	1.43	0.12	680	1.03	1.03	0.05	na	na	na	na	na	na	na	na
Jul	732	1.74	1.72	0.21	28	1.47	1.46	0.05	666	1.62	1.59	0.15	714	1.41	1.42	0.10	693	1.00	1.00	0.03	na	na	na	na	17	0.82	0.81	0.03
Aug	744	1.72	1.65	0.21	na	na	na	na	na	na	na	na	725	1.38	1.38	0.09	672	1.02	1.02	0.05	na	na	na	na	na	na	na	na
Sep	720	1.43	1.42	0.06	na	na	na	na	na	na	na	na	711	1.37	1.37	0.08	670	0.99	0.99	0.06	na	na	na	na	na	na	na	na
Oct	605	1.36	1.36	0.02	na	na	na	na	586	1.40	1.44	0.14	740	1.45	1.45	0.06	662	0.91	0.91	0.19	na	na	na	na	na	na	na	na
Nov	646	1.32	1.33	0.07	50	1.14	1.13	0.05	660	1.56	1.56	0.09	582	1.54	1.54	0.06	586	0.76	0.76	0.24	na	na	na	na	569	0.67	0.65	0.30
Dec	664	1.29	1.31	0.10	670	1.12	1.12	0.04	744	1.57	1.58	0.08	737	1.61	1.60	0.05	686	0.79	0.72	0.33	240	0.87	0.78	0.43	626	1.00	0.99	0.45
2015																												
Jan	na	na	na	na	na	na	na	na	730	1.56	1.56	0.10	139	1.57	1.57	0.04	648	0.94	0.83	0.41	710	0.88	0.81	0.51	711	0.82	0.82	0.31
Feb	na	na	na	na	na	na	na	na	665	1.52	1.50	0.14	560	1.58	1.59	0.06	520	0.95	0.92	0.25	652	0.93	0.78	0.59	664	0.81	0.81	0.21
Mar	na	na	na	na	na	na	na	na	701	1.53	1.58	0.19	585	1.47	1.46	0.09	na	na	na	na	734	1.50	1.47	0.31	695	0.90	0.89	0.09
Apr	na	na	na	na	na	na	na	na	707	1.39	1.48	0.37	607	1.56	1.54	0.15	na	na	na	na	717	1.49	1.49	0.16	715	0.89	0.88	0.06
May	na	na	na	na	672	1.05	1.01	0.37	742	1.34	1.34	0.23	741	1.47	1.48	0.08	na	na	na	na	648	1.31	1.30	0.11	329	0.90	0.89	0.05
Jun	na	na	na	na	387	1.22	1.21	0.16	616	1.67	1.64	0.20	703	1.49	1.48	0.09	na	na	na	na	717	1.20	1.18	0.06	na	na	na	na
Jul	na	na	na	na	na	na	na	na	720	1.73	1.70	0.20	729	1.50	1.50	0.09	na	na	na	na	744	1.14	1.14	0.05	na	na	na	na
Aug	na	na	na	na	na	na	na	na	682	1.53	1.54	0.12	568	1.54	1.52	0.12	na	na	na	na	740	1.10	1.10	0.07	na	na	na	na
Sep	na	na	na	na	na	na	na	na	616	1.67	1.64	0.20	703	1.49	1.48	0.09	na	na	na	na	718	1.03	1.05	0.15	na	na	na	na
Oct	na	na	na	na	na	na	na	na	707	1.37	1.37	0.07	665	1.52	1.51	0.05	714	0.94	0.96	0.21	725	0.71	0.69	0.32	na	na	na	na
Nov	na	na	na	na	na	na	na	na	682	1.40	1.41	0.08	568	1.48	1.49	0.05	695	0.91	0.90	0.26	680	0.54	0.48	0.29	na	na	na	na
Dec	na	na	na	na	na	na	na	na	702	1.52	1.51	0.11	628	1.46	1.46	0.09	712	0.91	0.79	0.41	598	0.81	0.76	0.33	na	na	na	na

Table 3: Monthly-based statistics (number of hourly-averaged Hg(0) data (n), mean, median, standard deviation (SD)) of Hg(0) concentrations (in ng m^{-3}) at ground-based Polar sites over the 2011-2015 period. Note that 2013 data at DC refer to concentrations recorded at 210 cm above the snowpack. na: not available due to QA/QC invalidation, instrument failure, or because the QA/QC validation is currently in progress (2015 data).

	GLEMOS			GEOS-Chem			GEM-MACH-Hg			ECHMERIT		
	NSE	RMSE	PBIAS	NSE	RMSE	PBIAS	NSE	RMSE	PBIAS	NSE	RMSE	PBIAS
ALT	0.12	0.29	4.9	0.32	0.25	1.3	0.49	0.22	4.1	-0.27	0.34	-10.0
SND	-0.83	0.29	-12.0	-0.85	0.29	-13.7	-0.17	0.23	-9.0	-2.85	0.42	-22.7
NYA	0.00	0.11	-6.3	-1.82	0.18	-9.7	-0.40	0.13	-4.4	-4.16	0.25	-15.5
AND	-2.76	0.20	-8.3	-2.50	0.19	-12.2	-0.26	0.12	-4.1	-6.24	0.28	-16.7
TR	-1.83	0.13	14.0	-4.76	0.19	3.0	-2.98	0.16	10.2	-2.50	0.15	-11.8
DC	-0.28	0.19	16.2	-1.07	0.25	7.5	-1.08	0.25	16.3	-0.32	0.20	-6.6
DDU	-6.10	0.24	25.4	-8.15	0.27	16.9	-4.87	0.22	16.7	-0.85	0.12	-5.1

Table 4: Goodness-of-fit statistics between monthly-averaged (year 2013) modeled and observed Hg(0) data at all ground-based sites: Nash-Sutcliffe efficiency (NSE, quantity without unit), root mean square error (RMSE, in ng/m^3), and percent bias (PBIAS, in %).

	GEOS-Chem				GEM-MACH-Hg			
	2011	**2012**	**2013**	**2014**	**2011**	**2012**	**2013**	**2014**
Summer								
ALT	-23.9	-1.9	-15.4	-17.1	-12.3	11.1	-9.2	-10.0
SND	34.3	-3.8	-22.0	4.6	11.6	1.4	-17.5	3.4
NYA	-8.9	-7.3	-14.7	-15.6	-5.9	-4.4	-0.2	-1.0
AND	-13.2	-10.4	-11.9	-14.1	-7.2	-6.8	3.2	3.0
TR	-1.1	-14.0	-8.9	-5.6	4.0	-1.9	6.3	23.6
DC	na	1.7	15.6	na	na	8.7	35.6	na
DDU	na	0.1	0.0	-8.3	na	-3.4	-1.7	8.4
Fall								
ALT	9.4	11.7	-9.8	-9.5	13.4	14.7	-3.6	-3.0
SND	-3.3	-1.5	-9.1	23.4	2.7	-0.5	-5.0	26.8
NYA	-11.1	-7.9	-14.4	-12.0	-9.3	-8.4	-9.7	-8.5
AND	-12.6	-11.1	-15	-12.1	-13.4	-12.5	-13.9	-6.5
TR	-13.1	-12.0	-10.9	-24.6	-7.8	-1.4	-2.9	-11.6
DC	na	-31.5	-22.6	na	na	-18.6	-43.4	na
DDU	na	-9.6	1.1	-19.9	na	-3.2	2.1	-4.4
Winter								
ALT	11.8	18.5	11.7	3.3	12.8	19.2	16.2	8.0
SND	5.5	5.5	4.2	11.6	5.1	4.8	5.5	15.3
NYA	4.1	0.1	-3.0	-4.0	1.3	-1.4	-1.4	-1.5
AND	-7.6	-9.0	-8.0	-7.6	-10.1	-11.1	-7.2	-6.7
TR	25.3	29.8	29.6	14.1	5.8	9.2	11.3	2.8
DC	na	79.9	39.3	na	na	48.4	17.8	na
DDU	na	38.5	50.4	49.4	na	15.4	26.9	40.4
Spring								
ALT	3.2	27.4	29.7	-21.8	-23.0	9.3	11.8	-24.0
SND	12.3	-11.6	-25.5	-33.3	4.2	-27.7	-23.0	-18.8
NYA	-5.8	-5.3	-9.7	-17.8	-23.8	-17.0	-21.5	-20.4
AND	-11.5	-13.8	-12.4	-16.7	-9.3	-16.0	-5.5	-7.6
TR	na	-9.0	13.0	-7.7	na	7.5	36.5	18.1
DC	na	32.6	22.9	na	na	48.8	34.5	na
DDU	na	3.2	73.6	na	na	31.9	62.8	na

Table 5: Percent bias (in %) between hourly-averaged modeled and observed Hg(0) data at all ground-based sites. Summer refers to Jun-Aug (Nov-Feb), fall to Sep-Nov (Mar-Apr), winter to Dec-Feb (May-Aug), and spring to Mar-May (Sep-Oct) at Arctic (Antarctic) sites. na: not available due to QA/QC invalidation, or instrument failure.

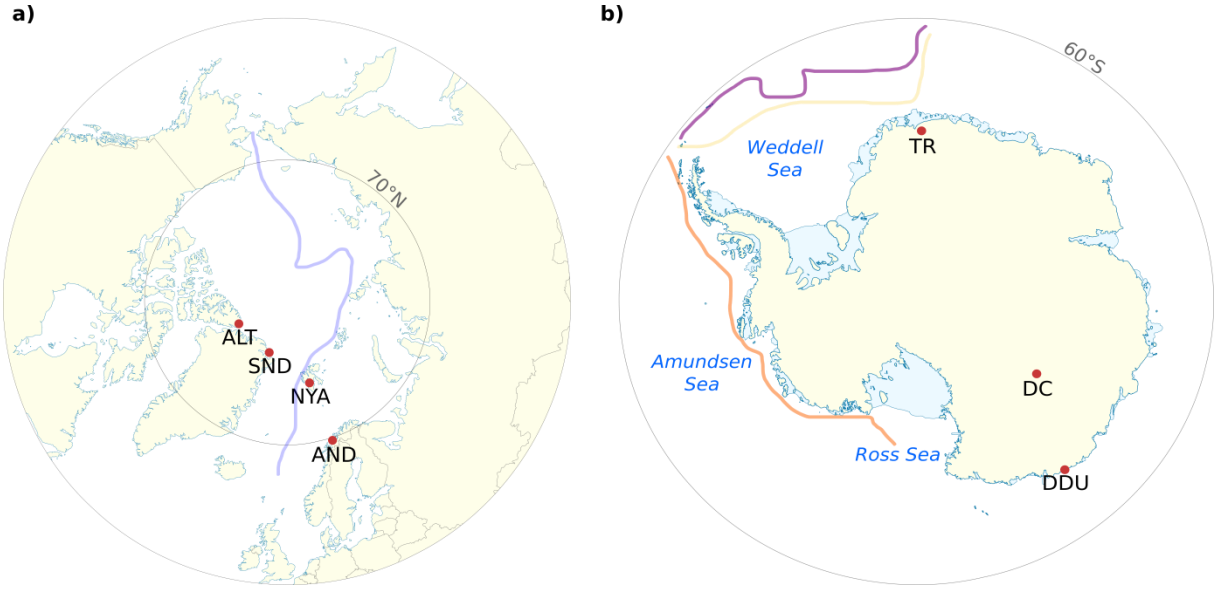

Figure 1: Location of **a)** Arctic and **b)** Antarctic ground-based sites whose data are reported in this paper: Alert (ALT), Villum Research Station at Station Nord (SND), Zeppelin station at Ny-Ålesund (NYA), Andøya (AND), Troll (TR), Concordia Station at Dome C (DC), and Dumont d'Urville (DDU). Additionally, the approximate path of cruises performed in recent years (2011-2015) is given: CHINARE 2012 in the Arctic onboard the Chinese vessel Xuelong (in blue), ANT XXIX/6-7 (denoted ANT in the paper) over the Weddell Sea onboard icebreaker Polarstern (in yellow and purple), and OSO 10/11 (denoted OSO in the paper) over Ross and Amundsen Seas onboard icebreaker Oden (in orange).

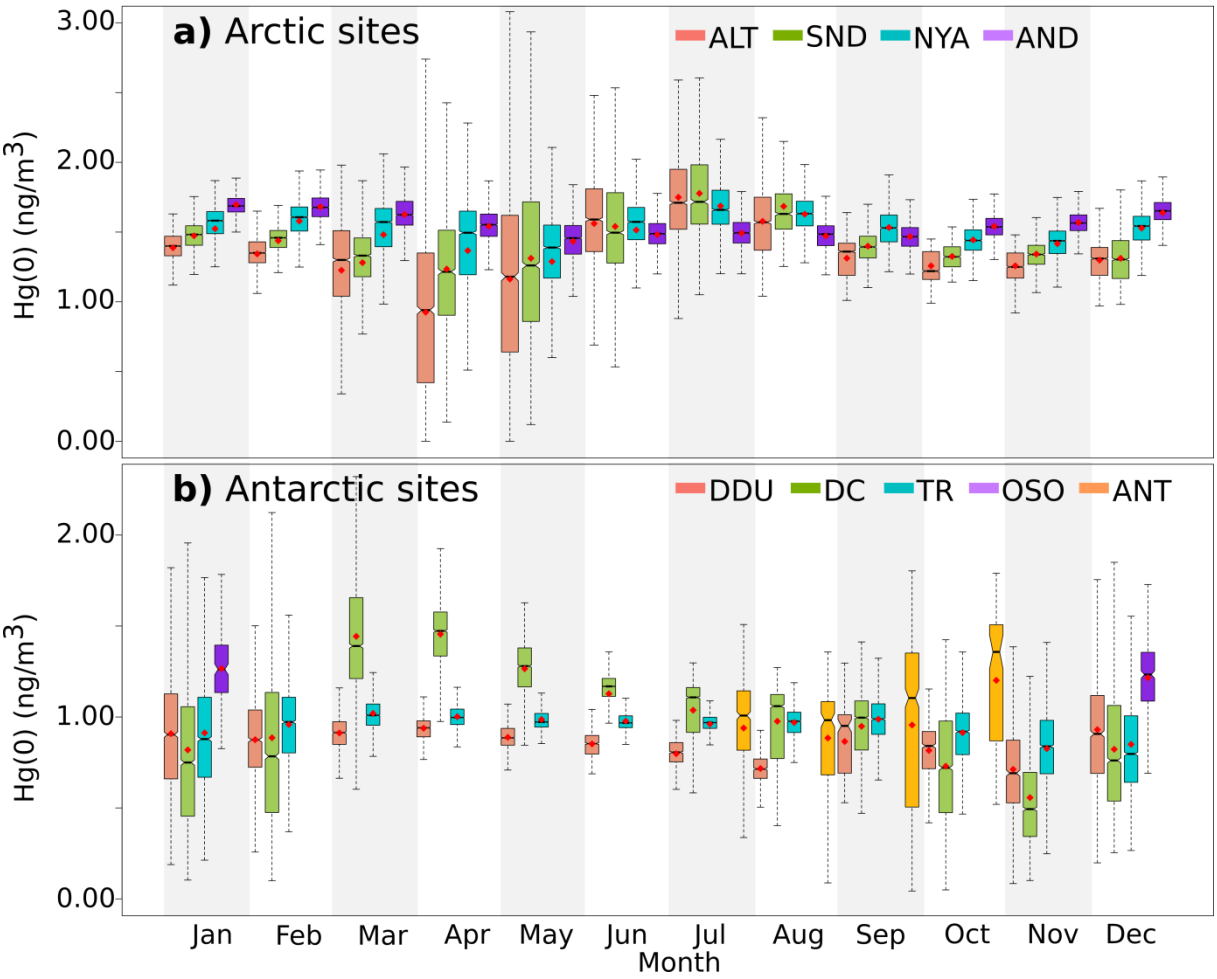

Figure 2: Box and whisker plots presenting the monthly Hg(0) concentration distribution at **a)** Arctic ground-based sites: ALT (red), SND (green), NYA (turquoise), AND (purple), and **b)** Antarctic sites: DDU (red), DC (green), TR (turquoise), during the OSO (purple) and ANT (orange) cruises. ◆: mean, bottom and top of the box: first and third quartiles, band inside the box: median, ends of the whiskers: lowest (highest) datum still within the 1.5 interquartile range of the lowest (upper) quartile. Outliers are not represented.

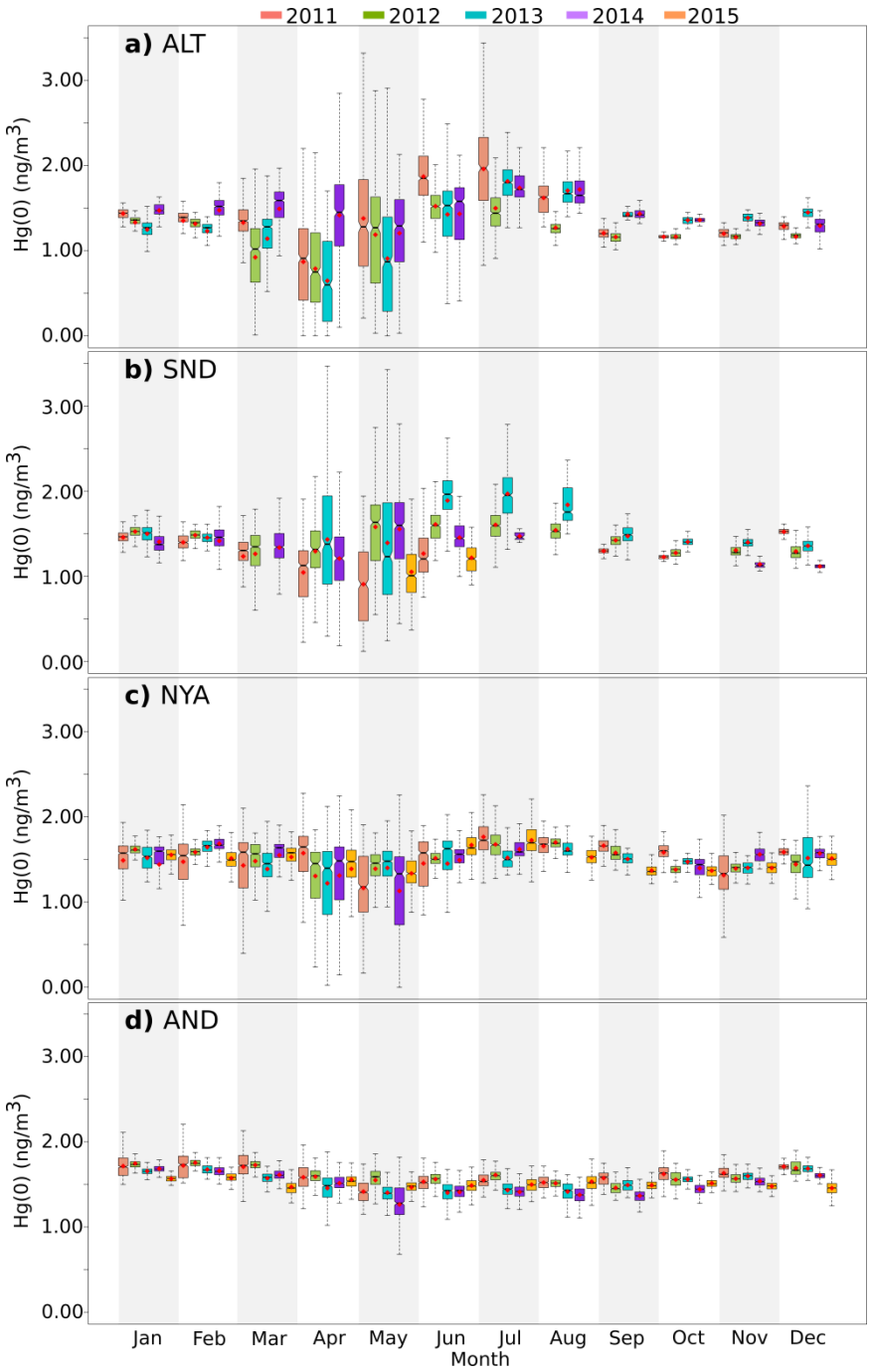

Figure 3: Box and whisker plots presenting the monthly Hg(0) concentration distribution at Arctic ground-based sites **a)** ALT, **b)** SND, **c)** NYA, and **d)** AND in 2011 (pink), 2012 (green), 2013 (turquoise), 2014 (purple), and 2015 (orange). ◆: mean, bottom and top of the box: first and third quartiles, band inside the box: median, ends of the whiskers: lowest (highest) datum still within the 1.5 interquartile range of the lowest (upper) quartile. Outliers are not represented.

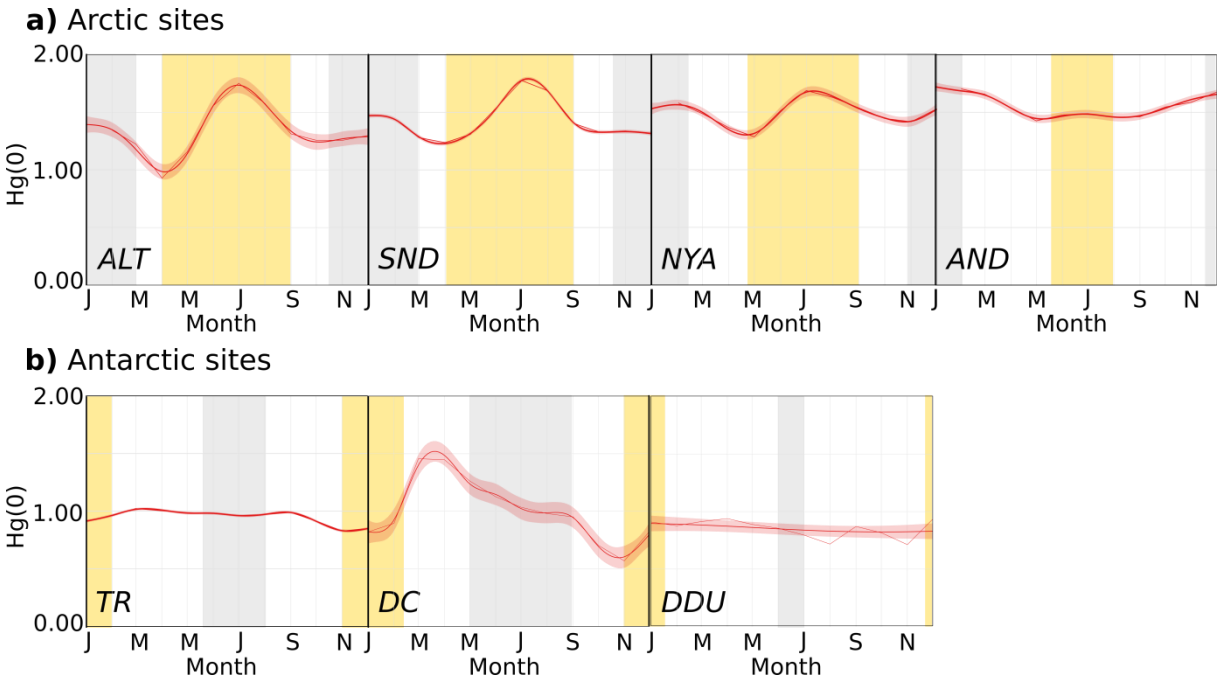

Figure 4: Seasonal variation (monthly mean along with the 95% confidence interval for the mean) of Hg(0) concentrations (in ng m^{-3}) at **a)** Arctic and **b)** Antarctic ground-based sites. Periods highlighted in yellow refer to 24-h sunlight and periods highlighted in grey to 24-h darkness. Summer refers to June-August (November-February), fall to September-November (March-April), winter to December-February (May-August), and spring to March-May (September-October) at Arctic (Antarctic) sites.

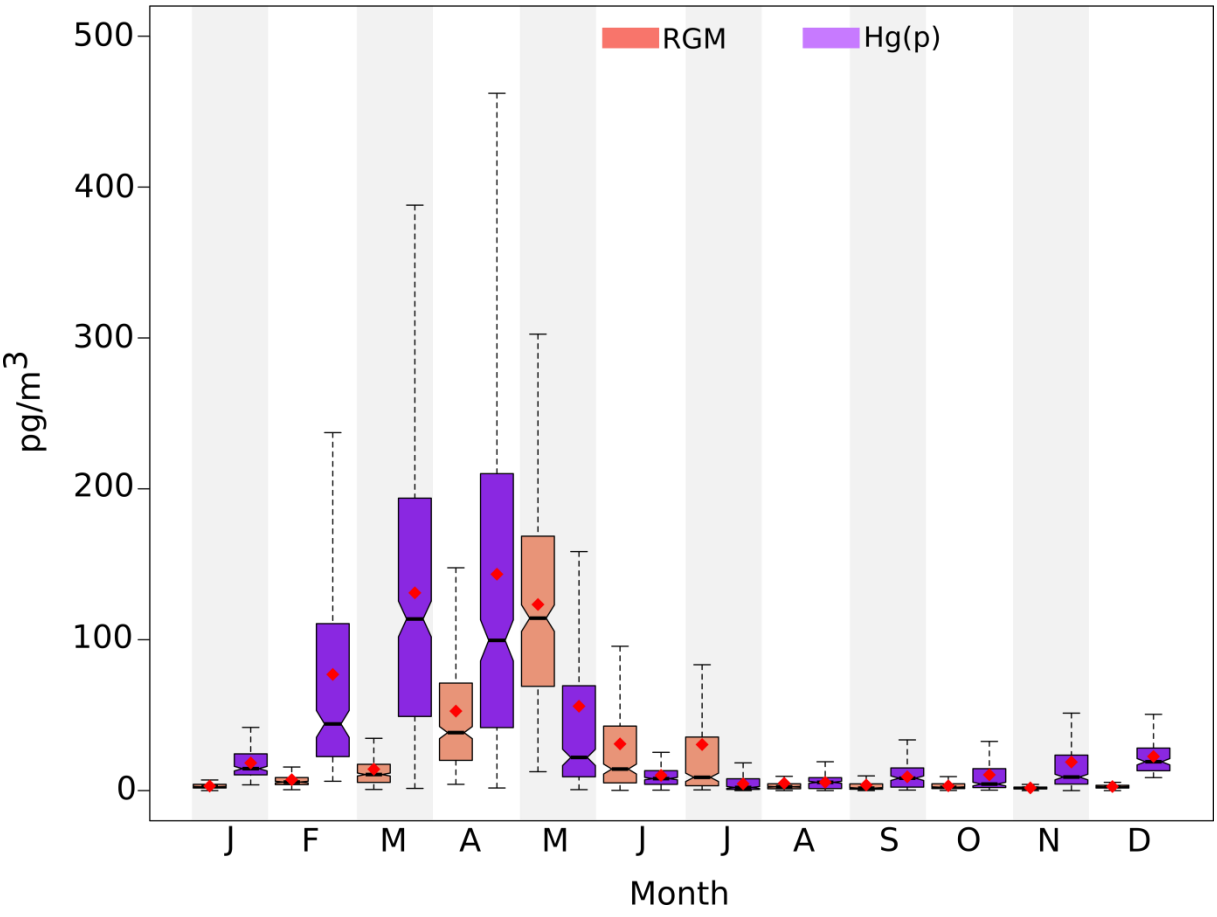

Figure 5: Box and whisker plots presenting the monthly RGM (in red) and Hg(p) (in violet) concentration distribution (in pg m^{-3}) at ALT over the 2011-2014 period. ◆: mean, bottom and top of the box: first and third quartiles, band inside the box: median, ends of the whiskers: lowest (highest) datum still within the 1.5 interquartile range of the lowest (upper) quartile. Outliers are not represented.

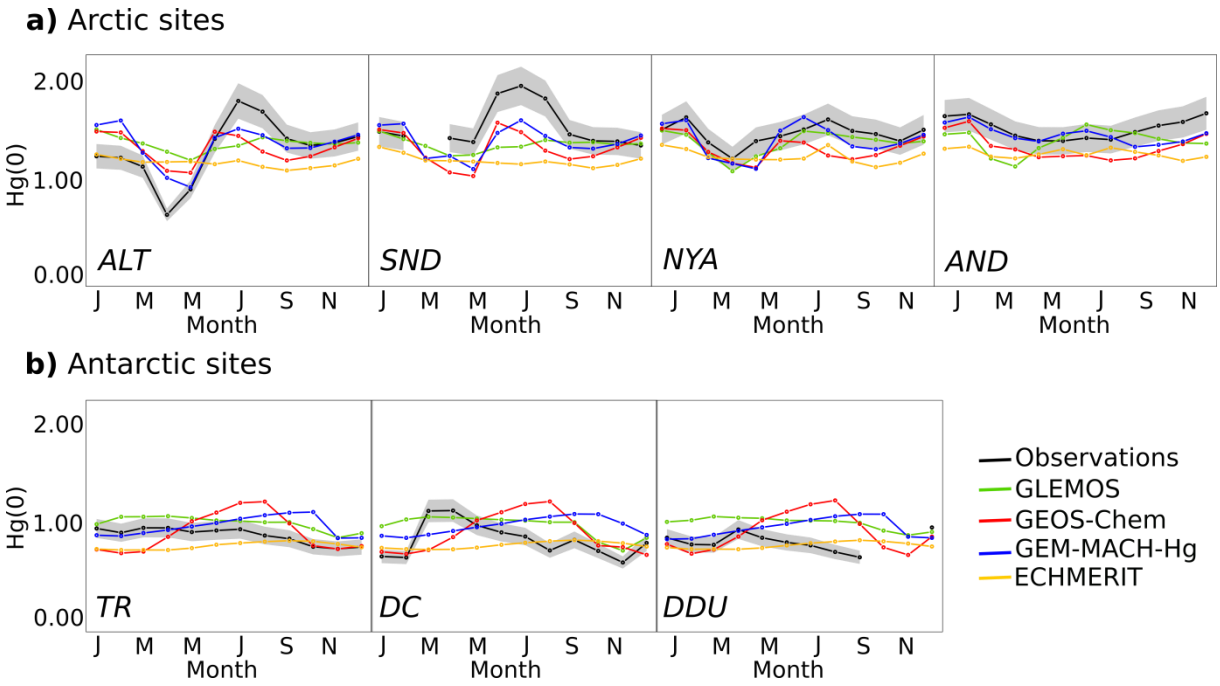

1703

1704 **Figure 6:** Year 2013 monthly-averaged Hg(0) concentrations (in ng m^{-3}) at **a)** Arctic and **b)**
1705 Antarctic ground-based sites: observations (in black) and concentrations according to the four
1706 global models (GLEMOS in green, GEOS-Chem in blue, GEM-MACH-Hg in red,
1707 ECHMERIT in yellow). The gray shaded regions indicate a 10 % uncertainty for
1708 observations.

1709

1710

1711

1712

1713

1714

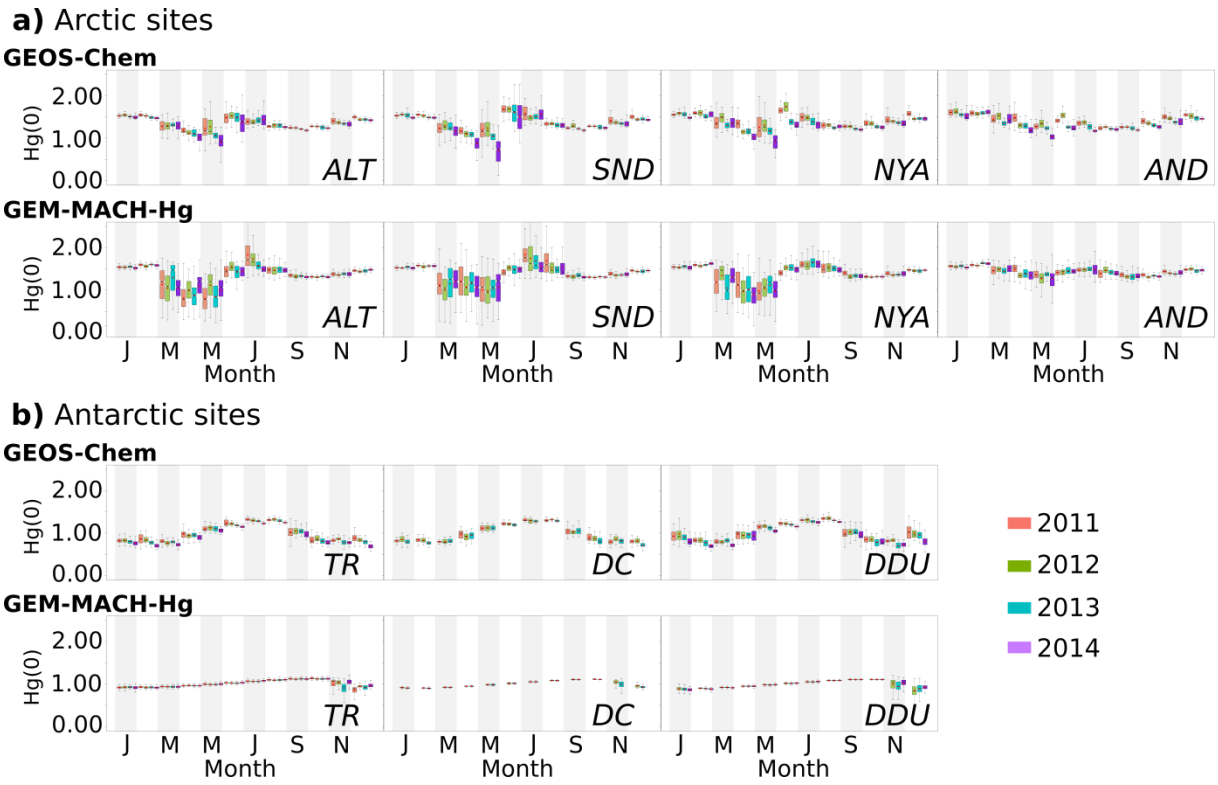

Figure 7: Box and whisker plots presenting the monthly Hg(0) concentration distribution at **a)** Arctic and **b)** Antarctic ground-based sites as simulated by GEOS-Chem and GEM-MACH-Hg in 2011 (pink), 2012 (green), 2013 (turquoise), and 2014 (purple). ◆: mean, bottom and top of the box: first and third quartiles, band inside the box: median, ends of the whiskers: lowest (highest) datum still within the 1.5 interquartile range of the lowest (upper) quartile. Outliers are not represented.

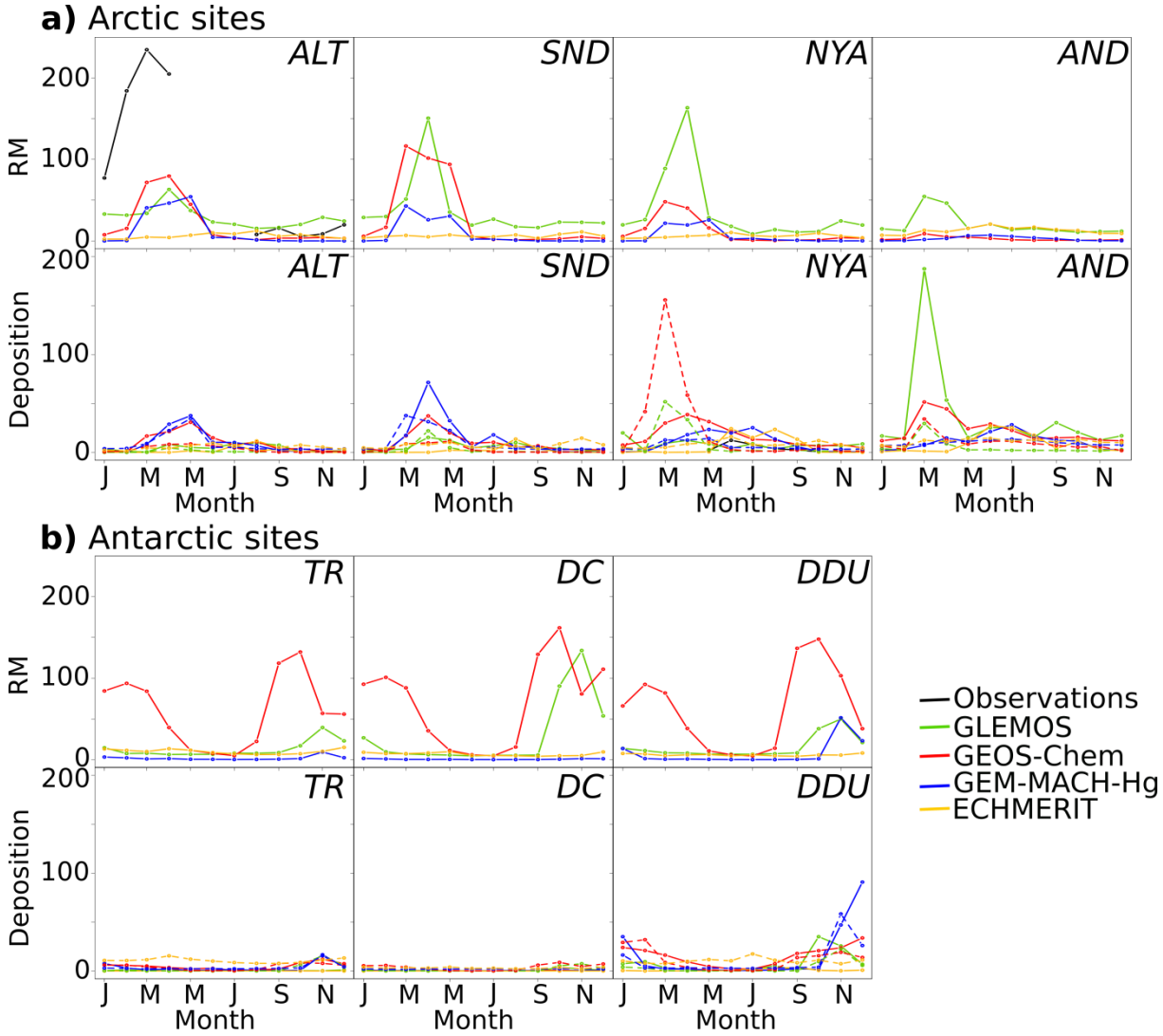

Figure 8: Year 2013 monthly-averaged mean reactive mercury (RM) concentrations (in pg m^{-3}) along with mean wet (solid line) and dry (dashed line) deposition (in ng m^{-2} day^{-1}) at **a)** Arctic and **b)** Antarctic ground-based sites: observations (in black) and concentrations according to the four global models (GLEMOS in green, GEOS-Chem in red, GEM-MACH-Hg in blue, ECHMERIT in yellow). Note that RM (wet deposition) observations are available at ALT (NYA) only.

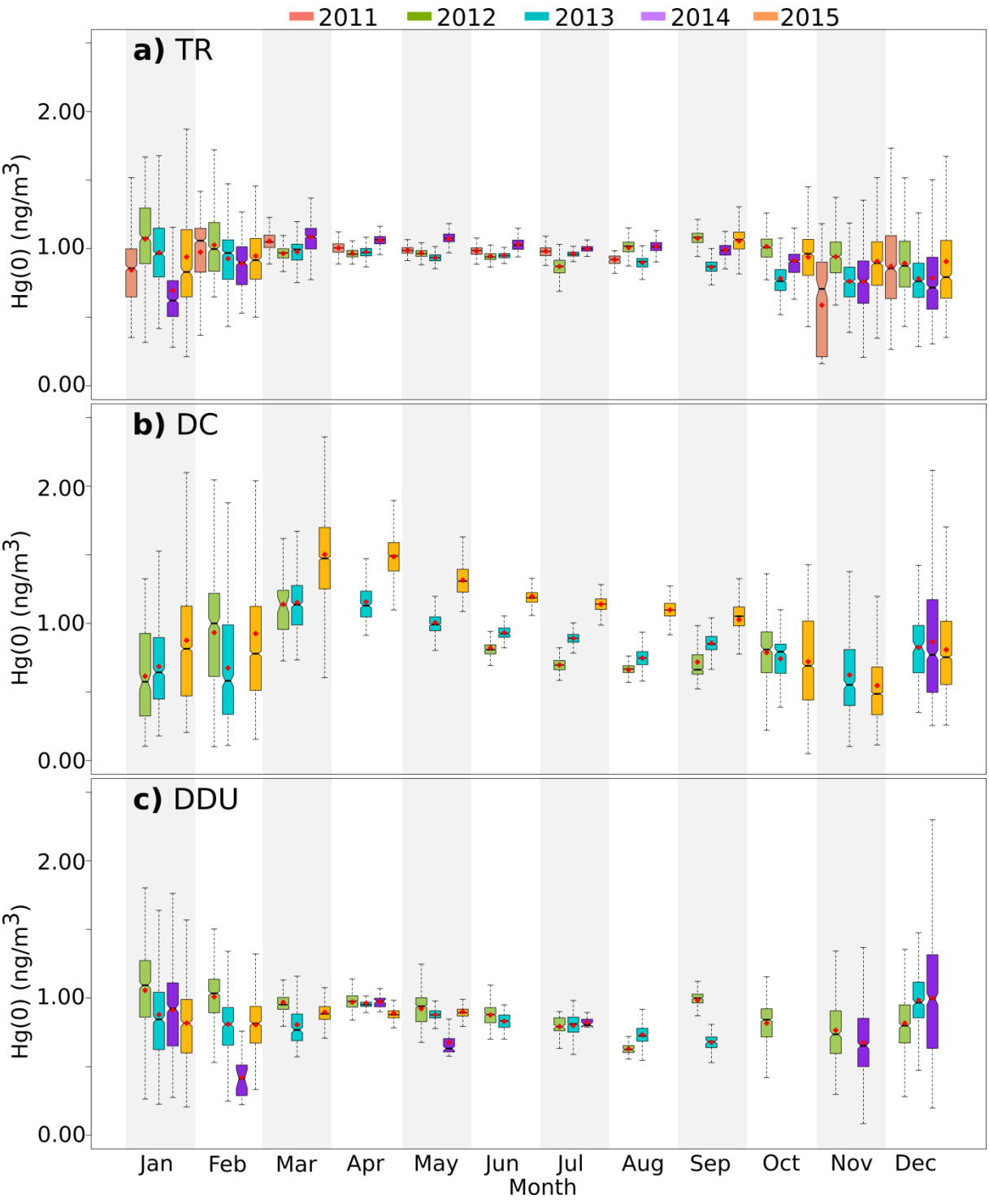

Figure 9: Box and whisker plots presenting the monthly Hg(0) concentration distribution at ground-based Antarctic sites **a)** TR, **b)** DC, and **c)** DDU in 2011 (pink), 2012 (green), 2013 (turquoise), 2014 (purple), and 2015 (orange). ◆: mean, bottom and top of the box: first and third quartiles, band inside the box: median, ends of the whiskers: lowest (highest) datum still within the 1.5 interquartile range of the lowest (upper) quartile. Outliers are not represented.